UNIVERSIDADE DE SÃO PAULO
ESCOLA DE ENGENHARIA DE LORENA

LUCAS CARVALHO TEIXEIRA

Design of a temperature sensor calibration setup

Lorena

2020

LUCAS CARVALHO TEIXEIRA

Design of a temperature sensor calibration setup

Versão Corrigida

Trabalho de conclusão de curso apresentado à Escola de Engenharia de Lorena da Universidade de São Paulo como requisito parcial para a conclusão do curso de Engenharia Física.

Supervisor: Dr. Luiz Tadeu Fernandes Eleno

Co-supervisor: Dr. Björn Bukkems

Lorena

2020

Ficha catalográfica elaborada pelo Sistema Automatizado
da Escola de Engenharia de Lorena,
com os dados fornecidos pelo(a) autor(a)

Teixeira, Lucas
Design of a temperature sensor calibration setup / Lucas Teixeira; orientador Luiz Eleno. - Lorena, 2020.
73 p.

Monografia apresentada como requisito parcial para a conclusão de Graduação do Curso de Engenharia Física - Escola de Engenharia de Lorena da Universidade de São Paulo. 2020

1. Design of a calibration tool. 2. Calibration of sensors. 3. Temperature sensor. 4. Lumped mass model. I. Título. II. Eleno, Luiz, orient.

To those who make this a fairer world

Acknowledgements

During the years of my education in the university, I have met so many amazing people. Indeed, the pages of this thesis could only be dedicated to blessed years, people and moments.

First of all, I want to thank my parents so much for always supporting my studies in an unbelievable way. Actually, not just my studies, but all my dreams. When I played soccer, they were there to support me. I studied 12 hours per day in order to enter university and they were there supporting me. I chose to live in an other city, they supported me. I have chose to live in a different country and they supported me. I have chose to travel around for 7 months and they supported me. Sure, not all of my decisions were easy on them, yet they were there supporting me. It means a lot to me. It changes everything.

I would like to express my appreciation to Ronald Timmermans. Even before I arrived in the Netherlands, Ronald Timmermans had already helped me a lot with many bureaucratic matters. Maybe without his work, patience and help I might not have had the opportunity to work on this project. This would have been a big disappointment for me. Thank you so much Ronald.

Thank you Björn Bukkems and Theo Ruijl for being my mentors. It was a long journey in which you two have led and taught me. Thanks for sharing your knowledge and for thinking about important subjects that I needed to learn during the project. A special thanks to Björn Bukkems who was working with me daily. I would like to say that your smile and question "How is life going?" in the beginning of our weekly meeting made a difference. Also, your support when the things were not going as expected during the project was helpful. And for being patient and kind about my English.

I used to say that friendship is the most important thing in life. My time in college confirms this. We study in one of the best universities of South America. However, I have no doubt that I have learned with my classmates what no teacher or any university could offer. The connection that we had was priceless and more than the connection classmates usually have, we were a big family.

My deepest appreciation to my housemates Daniel Ximenes and Giovani Teixeira. It is just impossible to express how grateful I am for having shared about 3 years of my life with you guys. It wasn't amazing, it was better, it was real. We didn't just laugh, we

also cried. Thank you Daniboy for plugging in the printer when I thought it was broken. Thank you for not judging my robot mode. Thanks for being yourself (the best) with me. Giovani, you use to say that I have changed your life. You are the change man. Thank you, Giovani, for listening me when my heart was broken. Thanks for sharing the worst period of the university with me. Thanks for being my brother. You are a gift in any life you appear, your kindness is limitless. We are most influenced by the five people we interact with most. Lucky me, I have been influenced by you guys.

Finally, I need to express my appreciation to Sonja Helena with whom I have worked to improve my writing skills. You are like a flower in a desert. In the middle of a pandemic you appear not just to help, but to share. Thanks for sharing not only writing skills, but also ideas, thought, fears, experiences and one hour of your day with me. I am deeply grateful for each single "class time".

"No rush...you will soon be dead"

Tim Minchin

Resumo

TEIXEIRA, Lucas C. **Projeto de um calibrador de sensores de temperatura**. 2020. 72 f. Dissertação (TCC) – Escola de Engenharia de Lorena, Universidade de São Paulo, São Paulo, Lorena, 2020.

Um grande número de sensores de temperatura é usado na análise de efeitos térmicos em sistemas de alta precisão. Por esse motivo, o projeto de um calibrador de sensores de temperatura teve início na empresa MI-Partners. O calibrador deve ser capaz de calibrar diferentes tipos de sensores em uma faixa de temperatura em torno de 10 °C – 50 °C com erro relativo de 1 mK. Todos os métodos de calibração são compostos por uma região de referência, um sensor de referência e um sistema de medição. A precisão da calibração aumenta com o aumento da homogeneidade térmica da região de referência. Portanto, desenvolver uma região de referência com alta homogeneidade térmica é um aspecto fundamental desse projeto. Para isso, um modelo conceitual foi idealizado a partir de conceitos fundamentais de transporte de calor. O modelo conceitual consiste de três cilindros concêntricos. O cilindro interno é a região de referência cuja temperatura precisa variar para a realização da calibração na faixa de temperatura definida, sem perder a alta homogeneidade térmica. O cilindro do meio é um isolante. E o cilindro de fora é um *shield* de alumínio. Além disso, água de um sistema de refrigeração circula por dentro do *shield*. Assim, o *shield* tem duas funções. A primeira função é reduzir perturbações térmicas. E a segunda é variar a temperatura da região de referência, como um atuador. O modelo conceitual foi modelado matematicamente (*Lumped Mass Model* - LMM) a fim de se calcular a espessura do isolante. A espessura ideal permite transferencia de calor suficiente para variar a temperatura da região de referencia, sem que ela perca sua homogeneidade térmica. Nesse processo, as dimensões dos cilindros foram definidas. Com isso, foi possível realizar uma segunda análise térmica por simulação via ANSYS. A homogeneidade térmica alcançada com LMM e com a simulação foi de 0.065 mK/mm e 0.066 mK/mm, respectivamente, que é quase dez vezes mais termicamente homogêneo que a homogeneidade térmica requerida de 0.5 mK/mm. A concordância entre resultados valida as análises e o projeto conceitual. A condição para obter esse resultado é que o *shield* seja isotérmico. Para satisfazer essa condição, o comportamento dinâmico desse subsistema (água-*shield*) foi analisado, uma vez que o fluxo de água dentro do *shield* atua sobre sua temperatura. Além disso, o desempenho do *shield* foi analisado para fluxo laminar e turbulento. A análise das fontes de erro do calibrador também foi feita. Soluções foram encontradas para algumas fontes de erro, no entanto, outras fontes de erro são intrínsecas ao sistema e não podem ser evitadas. A análise das fontes de erro mostrou que, entre os sensores estudados, aquele com a maior acurácia é o NTC 50K, cujo erro relativo varia de 0.5 mK até 1.2 mK para a faixa de temperatura de 10 °C to 50 °C.

Palavras-chaves: calibrador; sensores de temperature; lumped mass model

Abstract

TEIXEIRA, Lucas C. **Design of a temperature sensor calibration setup**. 2020. 72 p. Dissertation (Bachelor) – Escola de Engenharia de Lorena, Universidade de São Paulo, São Paulo, Lorena, 2020.

The analyses of thermal effects in high-precision systems requires a large number of high-accuracy temperature sensors. For this reason, the design of a temperature calibration tool started at MI-Partners. The calibration tool must be able to calibrate different types of sensors in a range of temperature of 10 °C to 50 °C with a relative error of 1 mK. Any calibration temperature method requires a reference region, a reference sensor and a measurement system. The precision of the calibration increases with the temperature homogeneity of the thermal reference region. Hence, designing a high-thermal-homogeneity reference region is a fundamental aspect in this project. Therefore, based on the fundamental concepts of heat transfer, a conceptual design has been created in order to obtain a thermal reference region with high homogeneity. The conceptual design consists of three concentric cylinders. The inner cylinder is the thermal reference region whose temperature must vary in order to do the calibration in the defined temperature range, without losing the high thermal homogeneity. The middle cylinder is an insulation. Finally, the outer cylinder is an aluminium shield. Along with this, water from a chiller circulates inside the shield. Thus, the shield has two functions. First, reducing thermal disturbances and, second, working as an actuator to change the temperature of the thermal reference region. The conceptual design was modelled via a lumped mass model in order to evaluate the thickness of the insulation. The ideal thickness allows enough heat transfer between the shield and the thermal reference region to vary the thermal reference region temperature, without losing its thermal homogeneity. From this process, the dimensions of the cylinders were defined. With this, it was possible to do a second thermal analysis of the system which was carried out using the ANSYS computational package. The temperature homogeneities achieved through the use of lumped mass modelling and simulation were 0.065 mK/mm and 0.066 mK/mm, respectively. These results are almost 10 times better than the requirement of 0.5 mK/mm. The agreement between these results validate the analyses and the conceptual design. The condition to obtain this result is that the shield should be isothermal. Since the water flow inside the shield changes its temperature, the dynamic behavior of this subsystem (water-shield) was analyzed in order to design the isothermal shield. Besides that, the shield performance was analyzed in the laminar and turbulent flows. In addition, the error analysis of the calibration tool was done. For some sources of error, solutions were found. However, some sources of errors are intrinsic to the system and do not have a solution. The error analysis showed that, among the studied sensors the most accurate temperature sensor is the NTC 50K, whose relative error varies from 0.5 mK to 1.2 mK for the temperature range of 10 °C to °50 C.

Keywords: calibration tool; temperature sensors; lumped mass modelling

List of Figures

List of Tables

List of abbreviations and acronyms

DMM	Digital Multimeter
DMME	Digital Multimeter Measurement Error
FEM	Finite Element Method
HTC	Heat Transfer Coefficient
ITS	International Temperature Scale
LMM	Lumped Mass Model
NTC	Negative Temperature Coefficient
PLC	Power Line Cycle
RTD	Resistance Temperature Detector
SHE	Self-Heating Error
TRR	Temperature Reference Region

Contents

1 Introduction

Accurate positioning is a fundamental requirement that determines the performance of several machines in the high-precision engineering sector, such as microscopes, machine tools, optical lithography machines, and many others. That is why the industry requirements for precision have becomes ever stricter. In order to realise this high accuracy, it is necessary to control the significant sources of errors.

There are several sources of error which decrease the accuracy of machinery, such as external and internal vibrations, measurement errors, and self-weight deformation. Besides these error sources, thermal effects are one of the most influential sources of error which lower the performance of high-end precision systems (BRYAN, 1990). Reducing these effects is not only important to accurate positioning, but also improves the repeatability and long term stability of machine tool and measuring equipment (LAMERS, 2014).

Besides high requirements for accuracy, the industry desires to keep increasing its productivity. In the case of increasing productivity requirements, thermal effects play an important role. For example, when one makes the machines work at a higher speed, more heat load enters the machine's structure. It will cause thermal expansion or drift which result in loss of accuracy. To solve this conflict, the high-tech industry has given priority to minimizing the thermal errors in the design of high precision systems over the last decade.

As defined by Morishima (2016, p. 19), "Thermal displacement errors in precision machines can be defined as the change of the relative distance between two points in a machine". This can occur in such examples as: a tool and a workpiece in a machine tool, a probe and the target in a measuring machine, or even a light source and the target in the microscopes or lithography machines. Thermal displacement errors are caused by heat load and heat transfer. The heat load can result from an actuator coupled in the machine or from variations in the environment temperature.

There are two types of thermal displacement errors:

1 - When there is no temperature gradient in the machine, but the machine's temperature is different from the nominal operating temperature. It means that the environment temperature is different from the machine's nominal operating temperature.

2 - When there is a temperature gradient in the machine structure.

Basically, in the first case, the machine's structure expands or shrinks and produces a shift at the point of interest. In the second case, the heat loads and the heat transfer produce some distributions in the temperature within the machine structure, resulting in more complex structural deformations.

Several approaches exist to minimize the thermal error, such as isolation of the heat source, reduction of the heat source, thermal shielding, thermal design, forced cooling, room temperature control, among others. (MORISHIMA, 2016). Based on Morishima (2016) and Koevoets et al. (2007), another approach would be to use the empirical Thermal Error Compensation Technique, which consists of finding a relationship between temperature distribution and deformation, i.e. a thermo-mechanical coupling. Therefore, by measuring the temperature in real-time, it is possible to predict the structure deformation and apply correction by controlling one part of the frame to correct any error caused by the deformation. The precision of this method depends on the accuracy of the thermo-mechanical coupling of the model.

To determine an accurate relationship between deformation and temperature, the use of a large number of high-accuracy temperature sensors is necessary, as illustrated in Figure 1. Due to this necessity, a temperature sensor calibration tool setup is desired by MI-Partners.

Figure 1 – Experimental set-up to analyze thermal effects

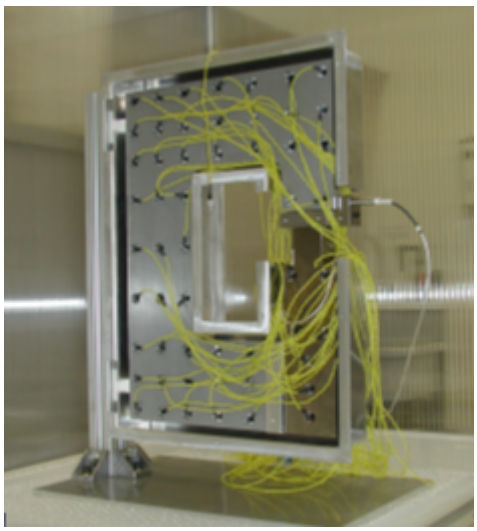

Source: Koevoets et al. (2007)

This thesis encompasses the complete design of a high-precision temperature sensor calibration setup. This project was divided into two phases: concept design and analysis of concept design. The conceptual design contains the explanation of the design choice

and the conceptual idea of the tool, whereas the analysis phase contains all the analyses necessary to verify if the concept design reaches the requirements of the project.

MI-Partners: Partners in Mechatronic Innovation is a Dutch company located in Eindhoven-Netherlands[1]. MI-Partners offers assistance in the development of high-precision mechatronic systems for customers (partners) worldwide. More specifically, this assistance can be divided in the parts of a project, such as:

- Feasibility study on mechanical, thermal or dynamical specifications and performance.
- Concept generation and design of a new machine.
- Realization of a prototype.
- Measurement and validation of specifications.

With such a workflow MI-Partners is able to provide assistance from specifications up to a fully functioning turn-key system. Within mechatronic systems, the main expertise areas of MI-Partners are: system architecture, design for precision, dynamics and control, thermal analysis and design, vibration isolation and damping, testing and validating, simulation and finite element method (FEM) analysis and project management among other. With this know-how MI has made many partners such as Philips, ASML, LNLS, Shell, Bosch, NXP, among others, since its foundation in 2007.

[1] Website of MI-Partners: http://www.mi-partners.nl/

2 Objective

In order to obtain high-accuracy temperature sensors, MI-Partners have established an internship project to design a temperature tool calibration setup. The present work, which has resulted from this project, does not cover any content about routine calibration or setting, nor does it contain aspects about calibration fitting techniques. The necessary information related to calibration in this thesis has been provided by members of the project team. The focus is to understand the physics and dynamics of the system to develop a consistent mechanical design of the tool.

The specific objectives of the calibration setup design were defined as follows:

- Calibration in the temperature range of 10 °C until 50 °C.
- Calibration absolute uncertainty of 3 mK.
- Relative error[1] of 1 mK.
- Temperature homogeneity of the thermal reference region better than 0.5 mK/mm.
- A system able to calibrate many sensors at the same type simultaneously.
- Calibration time of about 24 hours.

With the purpose to reach these specifications, the general objectives of this thesis are:

- Develop a conceptual design of the calibration tool.
- Define the parameters of the calibration tool.
- Verify if the requirements are feasible through modelling and simulation .

After the validation of the design, this project also includes the 3D drawing of the calibration setup.

[1] Relative error will be defined in section 5.3

3 Literature Review

Before going deep into the design aspects of the calibration setup, it is important to give a basic overview of the main characteristics of temperature sensors. It is also important to understand the calibration procedure, emphasizing the equipments and parts necessary to develop a calibration setup.

3.1 Temperature Sensor

Often it is not realized that it is impossible to measure temperature directly. All temperature measurements are indirect measurements. Usually, voltage, current, length and energy are measured and converted into temperature by some standard scale. Each one of these quantities is related to a specific sensor. In general, we can classify two types of temperature sensors: contact sensors, such as thermocouples, and non-contact sensors, such as an infra-red sensor. Due to the specific application of this project, the sensors of interest are the contact sensors: thermocouple, Resistance Temperature Detector (RTD), and Negative Temperature Coefficient (NTC).

Thermocouples consists of two wires of different metals welded at both ends, creating two junctions. If the junctions have different temperatures, a potential difference will appear between the two junctions, which is known as Seebeck Effect. Then, by holding the reference junction at a known temperature, it is possible to determine the sensing junction temperature via a voltage measurement. The big advantage of thermocouple is that they do not self-heat, which is a source of measurement error. However, it is not able to reach millikelvin (mK) resolution due to the signal/noise ratio (MORANTZ, 2016). RTDs and NTCs are resistance-based sensors. This means that both have the resistance as a function of the temperature $R(T)$, so the temperature can be evaluated by measuring the resistance. As these sensors are resistors, their big disadvantage is self-heating ($P = Ri^2$), where P $[W]$ is the power dissipated, R $[\Omega]$ is the resistance and i $[A]$ is the current. On the one hand, platinum RTD is the most common sensor among RTD sensors, due to their high stability. Moreover, this sensor has the best linearity. A disadvantage is that this sensor type has a high self-heating magnitude. On the other hand, NTCs are the most sensitive sensor type due to its exponential relation between resistance and temperature.

Furthermore, the self-heating effect is lower compared to the RTDs, because its work current is smaller. Table 1 summarizes the main sensors characteristics.

Table 1 – Main sensors characteristics

Characteristics	Thermocouple	RTD	NTC
Cost	Moderate	Moderate	Low
Stability	Poor	Best stability	Moderate
Noise Susceptibility	High	Low	Low
Self-Heating	None	High	Moderate
Output	Voltage	Resistance	Resistance
Sensitivity	Low	Moderate	Highest
Linearity	Highest	Logarithmic	Exponential
Temperature Range	$-270°C$ to $2300°C$	$-200°C$ to $650°C$	$-100°C$ to $300°C$

Source: Adaptaded from (LABFACILITY, 2006) and (MORANTZ, 2016)

3.2 Calibration Procedure Considerations

In general, calibration is a fundamental aspect of any instrument. It ensures that the instrument will work properly, and provides a means to quantify its uncertainty. In temperature sensors, uncertainties come from various factors, such as sensor resolution, measurement instrument inaccuracy, bad contact (sensor - probe), and self-heating. Furthermore, we must take into account that the accuracy of sensors are affected by many factors such as duration of use, as their performance decreases over time, temperature cycles and even contamination from external sources. All these factors result in an overall uncertainty of the system.

Calibration is the comparison between a measurement value from the non-calibrated device with a standard value or a value from another device which has a known accuracy (JCGM, 2008). Therefore, thermal calibration consists of placing the non-calibrated sensor on a known and controlled reference temperature region. Then by measuring the respective output (resistance or voltage), a correlation between correct temperature and measured value can be determined by curve fitting techniques to calibrate the sensor. Based on this, it is possible to define the parts and/or equipments required for a calibration system. A typical general-purpose system comprises:

- A thermal reference region (TRR)
- A certified high-accuracy sensor, which we will call the reference sensor, to verify the TRR's temperature.

- A high-precision measurement instrument

There are two calibration methods: comparison and fixed point. The fixed point method is based on the fundamental state of matter (such as is the triple, freezing, or melting point of some substances) defined by the International Temperature Scale (ITS90). The procedure of this method consist of placing the non-calibrated sensor in a fixed-point cell which contains one of the substances of the ITS90 at its fixed point. Then, the sensor can be calibrated with reference to a fixed point temperature. This method is the most accurate and provides a calibration against the absolute scale, which means that the calibration error is the absolute error. However, this method is limited to a small number of data points. For each data point it is necessary to restart the set-up by changing the fixed point cell with another substance. This procedure does not allow for an automation of the calibration. For these reasons, the method chosen for this project was comparison.

The comparison method, as the name implies, compares the measurement of the non-calibrated sensor with the measurement of the reference sensor. Both are placed in an isothermal reference temperature (liquid baths or dry-well are generally used). Based on the zeroth law of thermodynamics, if these three bodies are in thermal equilibrium, they will have the same temperature. In this case, it is possible to calibrate the sensor by comparing it with the reference sensor's temperature. In practice, it is difficult to ensure that the isothermal region is perfectly isothermal, or that the sensors will increase or decrease in temperature equally. In addition, one should note that the calibration error is not the absolute error, because the comparison is not related to a standard value which is considered the true value.

The content of this section is based on (ISOTECH, 2004) and (LABFACILITY, 2006).

3.3 Fundamental theory for the design of the calibration tool

The previous section highlighted the important aspects of temperature sensors and calibration methods for this project. For example, we have seen that a TRR with high thermal homogeneity is required in a calibration system. This subsection aims to review the fundamental concepts used to achieve the requirements and to design the calibration tool

set-up. The content of this section is based on (INCROPERA et al., 2007) and (CENGEL, 2007).

3.3.1 Conduction and Convection Heat Transfer Rates

There are several forms of energy and energy transfer processes. However, with regard to the design of a temperature sensor calibration tool, the form of interest is the energy transferred due to a spacial temperature difference. This is known as heat transfer. From the first law of the thermodynamics, heat transfer per unit of time can be expressed as

$$\dot{Q} = mc_p\dot{T} \tag{1}$$

where $\dot{Q}$ $[W]$ is the heat transfer rate, m $[kg]$ is the mass, c_p $[J/kg°C]$ is the specific heat capacity at constant pressure, which is the energy necessary to increase a unit of mass by one degree, and $\dot{T}$ $[°C/s]$ is the temperature rate.

There are three mechanisms of heat transfer, which are called modes: conduction, convection and radiation. Radiation is not relevant for this project and it will not be reviewed. The following is an explanation of the heat rate equation for conduction and convection, as well as their physical mechanisms responsible for the thermal energy transfer.

The interaction of atoms and/or molecules underlie the physical mechanisms of conduction. The basic idea is that the thermal energy passes from the more energetic particles to their less energetics neighbours via interaction. For this reason, conduction occurs in gases, liquids and solids. In gases and liquids, collision and diffusion are the causes of conduction. While in solids conduction is generally due to phonons (lattice vibrations), in the case of conductors free electrons also contribute to it. Mathematically, the thermal energy transferred per unit of time by theses processes can be evaluated using Fourier's law of heat conduction

$$\dot{Q} = -kA\frac{dT}{dx}. \tag{2}$$

k $[W/m°C]$ is the thermal conductivity which is a property of the material. This expresses the material capacity to conduct heat. If the material has high thermal conductivity, it will conduct heat quickly and easily. Whereas, if the material has low conductivity it will conduct heat slowly or less easily. The first are known as conductors, the latter, as insulators. The heat transfer area A $[m^2]$ is normal to the heat transfer direction. $\frac{dT}{dx}$ is

the gradient of temperature in the x direction. Finally, the negative sign ensures that heat flows from the higher temperature to the lower temperature.

The two physical mechanisms of convection are diffusion and fluid motion. Convection may be understood as the heat transfer between a fluid in motion and the surface of a solid, both at different temperatures. Clearly, convection is strongly influenced by the fluid flow and can be classified in relation to it. If the fluid is accelerated against the solid surface by external means, such as through the use of a pump or fan, the flow is termed forced convection. When the flow is created by buoyancy forces, caused by density differences, due to the temperature gradient in the fluid, the convection is termed free or natural convection. The rate of convection heat transfer is determined by Newton's law of cooling as

$$\dot{Q} = hA(T_s - T_\infty) \tag{3}$$

where h $[W/^\circ Cm^2]$ is the convection heat transfer coefficient (HTC), A $[m^2]$ is surface area of the solid which exchanges heat with the flow, T_s $[^\circ C]$ is the temperature of the surface of the solid, and T_∞ $[^\circ C]$ is the temperature of the fluid far away from the surface. In many cases the heat flux and the HTC vary along the surface. In such cases, one might be interested in the total convection heat transfer ($\dot{Q}_t$), given as

$$\dot{Q}_t = \overline{h}A_s(T_s - T_\infty) \tag{4}$$

where $\overline{h}$ is the average heat transfer coefficient.

The simplicity of Equation 3 does not express the complexity of convection heat transfer analysis, because it does not evince the challenge of calculating the HTC. Unlike thermal conductivity, the HTC is not just a property of the flow. Indeed, as Incropera et al. (2007, p.8) states "any study of convection ultimately reduces to a study of the means by which h may be determined."

3.3.2 Dimensionless Parameters

The convection heat transfer coefficient depends on several fluid properties (such as density, viscosity, thermal conductivity and specific heat), surface geometry and flow conditions. Due to the large number of variables, it is difficult to determine HTC. For this reason, in convection problems, dimensionless parameters are usually used in order to reduce the large number of variables. This practical approach normally permits evaluating

HTC using empirical relations. In the following, the dimensionless parameters relevant to this project are defined and interpreted physically. In addition, the equations of these dimensionless parameters for flow in pipes are discussed.

Reynolds number (Re)

The flow conditions have high relevance in the study of convection heat transfer. Among the different flow conditions are: compressible or incompressible, natural or forced, steady or unsteady. We are particularly interested in the regime condition of the flow, which can be laminar or turbulent. The laminar flow is characterized by smooth streamline which has an ordered motion, while the turbulent flow is characterized by chaotic streamline which has an high-disorder motion. Moreover, the transition between laminar and turbulent flow does not occurs suddenly. Actually, there is a transition regime in which the flow fluctuates between laminar and turbulent. This transition depends on numerous factors, such as surface geometry, surface roughness, surface temperature and type of fluid, among others. However, it is not necessary to analyze all these factors, because the dimensionless parameter Re is enough to determine the regime of the flow. The Reynolds number can be viewed as the ratio of the inertia forces ($F_I \simeq V^2/L_c$) to viscous forces ($F_s \simeq \nu V/L_c^2$) in a region of characteristic dimension L_c. Thus, the Reynolds number is

$$\frac{F_I}{F_s} = \frac{V^2/L_c}{\nu V/L_c^2} = \frac{\rho V L_c}{\mu} = Re_L \tag{5}$$

where V $[m/s]$ is the flow velocity, $\nu = \frac{\mu}{\rho}$ $[m^2/s]$ is the kinematic viscosity of the fluid, and where μ $[N.s/m^2]$ is the dynamic viscosity and ρ $[kg/m^3]$ is the density. When Re is low, the viscous forces are predominant, which results in a laminar flow. However, when Re is high the inertia forces, which are proportional to the velocity, are stronger than the viscous forces. Hence, the viscous forces cannot prevent the chaotic and disordered motion of the fluid. Consequently, there is turbulent flow when Re is high. The limit Re, in which the flow starts to become turbulent, is known as the critical Reynolds number. Regarding the flow in pipes the critical Reynolds number is $Re_c = 2300$, although to achieve fully turbulent flow a much larger Re is needed ($Re_c \simeq 10000$).

Regarding the flow in pipes, the characteristic dimension is the effective diameter, called the hydraulic diameter (D_h), which is defined as

$$D_h = \frac{4A_c}{P} \tag{6}$$

where A_c $[m^2]$ is the flow cross-section area and P $[m]$ is the "wetted perimeter". In the case for circular pipes, D_h is equal to the diameter of the pipe. Moreover, it is important

to note that with D_h, it is possible to calculate dimensionless numbers for non-circular pipes. Thus, the Reynolds numbers for pipes is given by

$$Re_{D_h} = \frac{\rho V D_h}{\mu} \tag{7}$$

Prandtl number (Pr)

Prandtl number is defined as the ratio of the momentum diffusivity ν to the thermal diffusivity α

$$Pr = \frac{\nu}{\alpha} \tag{8}$$

In practice the Prandtl number used is given by tables for specific temperatures. The values of Pr range from 0,01 for liquid metals to more than 100 000 for oils. This number measures which kind of dissipation is predominant, i.e. heat or momentum based.

Friction factor (f)

The friction factor is essential in any study of heat transfer by convection, because it is directly related to the HTC. In addition, the friction factor is the main parameter which determines the power of the pump or fan that the system needs. For flow in pipes, the friction factor for fully developed laminar flow is given by

$$f = \frac{64}{Re_{D_h}} \tag{9}$$

For the turbulent flow, the equation is much more complex, because in this regime the friction factor depends on the Re and the relative roughness of the surface (ϵ/d), where ϵ is the roughness and d is the diameter of the pipe.

$$\frac{1}{f^{1/2}} \simeq -1.8\ log\left[\frac{6.9}{Re_{D_h}} + \left(\frac{\epsilon/d}{3.7}\right)^{1.11}\right] \tag{10}$$

This equation works for smooth and rough pipes and for a large range of Reynolds numbers. However, there is no reliable friction factor in this range, $2000 \lesssim Re_D \lesssim 4000$ (WHITE, 2007). A practical alternative to determine f in the turbulent region is to use the Moody diagram (INCROPERA et al., 2007, p. 491).

Nusselt number (Nu)

Another important dimensionless parameter is the Nusselt number which in many cases can be used to calculate the heat transfer coefficient. To understand the physical interpretation of the Nusselt number, consider a layer of fluid with thickness L, in which there is a temperature difference of ΔT. As a result, on the one hand, if the fluid has motion, heat

transfer will occur by convection ($\dot{Q}_{conv} = A_c h \Delta T$, which comes from Eq. 3). On the other hand, if the fluid has no motion, heat transfer will occur by conduction ($\dot{Q}_{cond} = A_c k \Delta T / L$, which comes from Eq. 2). The Nusselt number can be viewed as the ratio of convection to pure conduction in a fluid.

$$\frac{\dot{Q}_{conv}}{\dot{Q}_{cond}} = \frac{A_c h \Delta T}{A_c k \Delta T / L} = \frac{hL}{k} = Nu \tag{11}$$

The larger the Nusselt number, the higher the convection is in relation to conduction. Thus, the Nusselt number is a way to measure the convection heat transfer occurring at the surface.

For flow in pipes the Nusselt number depends on the flow regime. With laminar flow for constant surface temperature, the Nussel number is

$$Nu_{D_h} = 3.66 \tag{12}$$

For turbulent flow the Nusselt number is given by a much more complex equation, which is

$$Nu_{D_h} = \frac{(f/8)(Re_D - 1000)Pr}{1 + 12.7(f/8)^{1/2}(Pr^{2/3} - 1)} \tag{13}$$

where f can be evaluated by equation 13. This correction is valid for $0.5 \lesssim Pr \lesssim 2000$ and $3000 \lesssim Re_D \lesssim 5.10^6$.

3.3.3 Lumped mass model (LMM)

The lumped mass model is highly recommended for the analysis of thermal systems due to its versatility and fast results (RUIJL, 2011). This modelling consists of using state-space representation with the appropriate heat transfer equations and the concept of lumped systems.

Thermal resistance concept

First of all, the concept of thermal resistance must be introduced. Let's consider conduction through a plane wall with thickness L. The temperature difference between both surfaces is $\Delta T = T_2 - T_1$. The heat transfer rate through the wall can be calculate from Equation 2 as

$$\int_0^L \dot{Q} dx = -kA \int_{T_1}^{T_2} dT$$

$$\dot{Q} = \frac{kA}{L} \Delta T$$

Rearranging it, we get

$$\Delta T = \frac{L}{kA}\,\dot{Q} \tag{14}$$

In this form, comparing Equation 14 to the known Ohm's law equation $\Delta U = R.I$, it is clear that $\frac{L}{kA}$ can be interpreted as the resistance that the heat flow experiences passing through the wall. Thus,

$$R_{cond} = \frac{L}{kA} \tag{15}$$

Using the same reasoning, the resistance for convection can be derived from equation 3, which results in

$$R_{conv} = \frac{1}{hA} \tag{16}$$

The thermal resistance concept allows to model and analyze a variety of steady and transient one-dimensional heat transfer problems.

Lumped systems concept

As the name implies, this concept suggests that parts of a body behave as "a lump". This means that the parameters of interest of the body do not vary spatially. With regards to this project, in such cases, the temperature of the body can be analyzed as a function of time $T(t)$. Normally, this idealization, can be used for materials of high thermal conductivity, since for them the thermal resistance can be small and the heat disperses quickly, keeping the temperature throughout the body constant. Nevertheless, an appropriate criterion to know if the lumped mass analysis can be used, is to evaluate the Biot number (Bi). This is the ratio of the thermal resistance of the body (conduction) to the thermal resistance of the surrounding convection. It can be expressed as

$$Bi = \frac{R_{cond}}{R_{conv}} = \frac{\frac{L}{kA}}{\frac{1}{hA}} = \frac{hL}{k} \tag{17}$$

where $L = \frac{V}{A_s}$ is the characteristic length, defined as the volume of the body, divided by its surface area.

The Biot number is a measure of the effectiveness of the conduction within the body against the heat transfer by convection from the outside. It is generally accepted that a element can be treated as a lumped element if

$$Bi \leq 0.1 \tag{18}$$

In this case the temperature gradient within the body can be considered negligible. This criterion has been presented for the completeness of the lumped mass concept. However,

this criterion has not been used in the analyses of this project since here we are not going to deal with the interplay between conduction in solid and convection in a fluid.

Thermal Modelling

Generally, the first step in modelling is to transform the real system or concept into a block diagram model. An example of thermal modelling, as applied in this project, is given in Figure 2, where $m1$, c_{p1}, T_1 and $m2$, c_{p2}, T_2 are the mass, the specific heat and the temperature of the bodies 1 and 2 respectively. This topic is based on (RUIJL, 2012).

Figure 2 – Model example

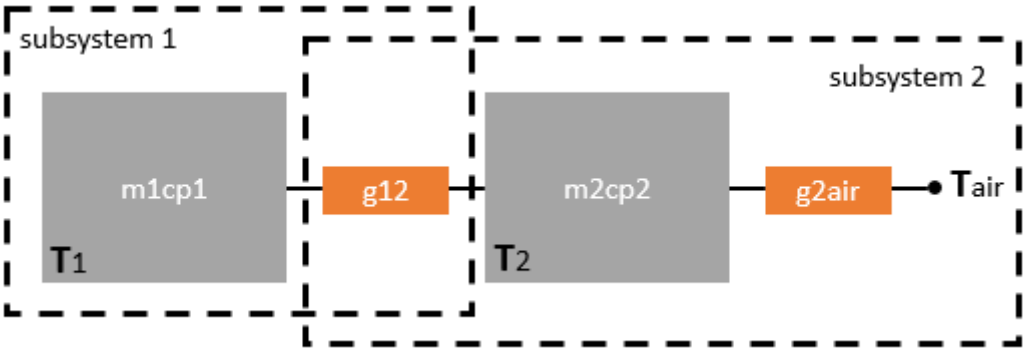

Source: Author

Note that for thermal modelling, instead of using resistances, it is more convenient to use $g = 1/R\ [W/K]$ which we will term heat conductivity. Therefore, in Figure 2, g_{12} is the heat conductivity between the two bodies and g_{2air} is the heat conductivity between body 2 and the air at temperature $Tair$.

All heat transfer rate equations of each subsystem of the model must be formulated. The negative heat flow is considered to leave the mass, such that $\dot{Q} = g(T_{end} - T_{mass})$. In case of heat load into the mass it is considered positive, since it increases the body temperature.

Hence, for subsystem 1 in Figure 2

$$m_1 c_{p1} \frac{dT_1}{dt} = \sum \dot{Q}_1$$
$$\sum \dot{Q}_1 = g_{12}(T_2 - T_1)$$

Which results

$$m_1 c_{p1} \frac{dT_1}{dt} - g_{12} T_2 + g_{12} T_1 = 0 \tag{19}$$

Doing the same for subsystem 2

$$m_2 c_{p2} \frac{dT_2}{dt} = \sum \dot{Q}_2$$
$$\sum \dot{Q}_2 = g_{12}(T_1 - T_2) + g_{2air}(T_{air} - T_2)$$

Which results

$$m_2 c_{p2} \frac{dT_2}{dt} + (g_{12} + g_{2air})T_2 - g_{12}T_1 = g_{2air}T_{air} \tag{20}$$

The next step is to write equations 19 and 20 in the matrix form as

$$\begin{bmatrix} m_1 c_{p1} & 0 \\ 0 & m_2 c_{p2} \end{bmatrix} \begin{bmatrix} \dot{T}_1 \\ \dot{T}_2 \end{bmatrix} + \begin{bmatrix} g_{12} & -g_{12} \\ -g_{12} & (g_{12} + g_{2air}) \end{bmatrix} \begin{bmatrix} T_1 \\ T_2 \end{bmatrix} = \begin{bmatrix} 0 \\ g_{2air} \end{bmatrix} \begin{bmatrix} T_{air} \end{bmatrix} \tag{21}$$

which can be written as

$$\mathbf{E}\vec{\dot{T}} + \mathbf{K}\vec{T} = \mathbf{L}\vec{u} \tag{22}$$

where $\mathbf{E}$ is the heat capacity matrix, $\mathbf{K}$ in the heat transfer matrix and $\mathbf{L}$ is the heat load matrix. Finally, it is possible to write the lumped mass equation in the state-space description

$$\begin{cases} \vec{\dot{T}} = \mathbf{A}\vec{T} + \mathbf{B}\vec{u} \\ \vec{T} = \mathbf{C}\vec{T} \end{cases}$$

where the matrices $\mathbf{A}$, $\mathbf{B}$ and $\mathbf{C}$ are $\mathbf{A} = -\mathbf{E}^{-1}\mathbf{K}$, $\mathbf{B} = -\mathbf{E}^{-1}\mathbf{L}$ and $\mathbf{C} = \mathbf{I}$ (if all temperatures are desired as output), respectively.

By solving this system of equation the temperatures of body 1 and 2 in Figure 2 can be determinated. The goal of this example is to demonstrate how to model a lumped mass system as it was done in this project.

4 Design Consideration and Conceptual Design

The accuracy of comparison calibration increases as the temperature of the non-calibrated sensor and the reference sensor get closer to being equal to each other. This depends on the temperature homogeneity of the TRR. In other words the accuracy of the comparison calibration increases as the temperature homogeneity of the TRR increases. This means that the fundamental aspect of this design is to ensure that the TRR's temperature is homogeneous as required. However, a perfect homogeneous region is impossible to achieve because one needs to vary the temperature of the TRR in order to perform the calibration in a range of temperatures. To change the TRR's temperature, a heat flow is needed, and because of this, a temperature gradient exists. For this reason, the heat flow into the TRR needs to be small to obtain a good temperature homogeneity, but at the same time it needs to be large enough to change the TRR's temperature within the calibration time of twenty-four hours.

Therefore, the thermal design can be tackled by:

1. Reducing the heat flow into the TRR
2. Optimizing the system design to avoid thermal disturbances.

With (1) the goal is that the system can be able to change the TRR's temperature and, simultaneously, keep the homogeneity better than 0.5 mK/mm. Moreover, (2) ensures that any thermal disturbance, such as fluctuations in the temperature of the environment, and others do not affect the homogeneity of the thermal reference region.

4.1 Insulation

In our daily life, several examples of reduction of heat flow can be found. For example, a winter jacket or a blanket minimizes the heat flow from our body to the environment. Alternatively, a thermal bag avoids heat exchange between the inside and the outside. More sophisticated applications in high precision machines, such as insulation of electronic components, are well described in Ruijl (2001). In summary, insulators are widely used and it is an effective way to reduce heat flow.

Applying this well known concept to the design of the calibration tool, a material with low thermal conductivity should be placed between the TRR and the temperature

source, such that the heat flow into the TRR can be reduced by the insulation. Note that there is a trade-off related to this. On the one hand, it is important to have sufficient coupling between the temperature source and the TRR in order to have a quick system response. On the other hand, in the case of a good coupling, any disturbance, such as environmental disturbances, would also have a good coupling with the TRR.

Despite the fact that there are various options of insulation materials, as shown in Figure 3, foam has been chosen as an insulator because of two main reasons. First, the low conductivity and density of the foam result in a compact and lightweight calibration tool. Second, it can act as a support for the thermal reference region.

Figure 3 – Thermal conductivity of different materials

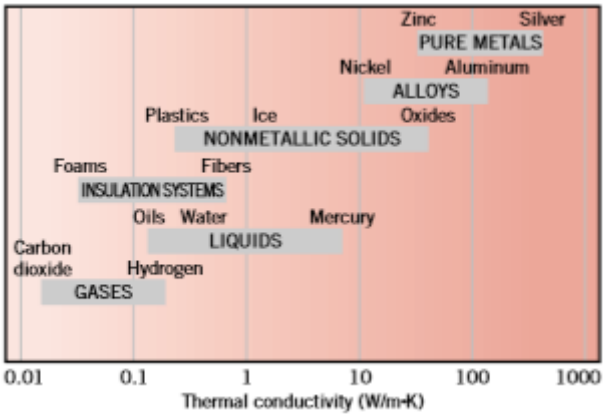

Source: Incropera et al. (2007)

4.2 Thermal Reference Region (TRR)

As mentioned, the crucial aspect of this design is to ensure that the non-calibrated sensor and calibrated sensor measure the same temperature. It means that the thermal reference region must have high temperature homogeneity.

In this case, materials with high thermal conductivity should be used, because the heat flows quickly in these materials, minimizing the temperature gradient. An alternative way to understand it is to analyze Equation 2. Since $\dot{Q}$ is required to change the TRR's temperature, a material with high conductivity k decreases the temperature temperature gradient $\frac{dT}{dx}$, which is the same as increase the temperature homogeneity. Therefore, based on Figure 3 the best choice for the material of the TRR is a pure metal.

The metals with higher conductivity are silver 429 [W/m.K], copper 400 [W/m.K], gold 317 [W/m.K] and aluminum 237 [W/m.K] (INCROPERA et al., 2007). Due to the high cost, silver and gold are excluded.

In addition, larger body masses result in slower temperature variation. This increases the calibration time, which needs to be avoided since the insulation will already contribute to increasing the calibration time. This means that a good way to select the material for the thermal reference region is to research a material with large conductivity over density ratio $\frac{k}{\rho}$, which can be use to decide between copper and aluminum. Hence, $\frac{K_{Cu}}{\rho_{Cu}} = 0.044$ for copper and $\frac{K_{Al}}{\rho_{Al}} = 0.087$ for and aluminum . It is possible to conclude that the best material to use as the TRR is aluminum. All property values used in the previous calculations refer to the temperature at 25 $°C$.

4.3 Shield

Shielding has been used to minimize thermal effects in precision systems (RUIJL, 2011)(RUIJL, 2001). Figure 4 shows that the room's temperature fluctuations are almost eliminated by the aluminum shielding and the enclosure. In Ruijl (2011, p. 3) it is stated that "the high thermal conductivity of aluminum significantly decreases the effects of local heat sources". To understand this, the same reasoning, that materials of high conductivity avoid temperature inhomogeneity discussed in the previous section, is applied here. In other words, the shield provides an isothermal surrounding for the frame.

This idea can be used to protect the TRR against thermal disturbances. Therefore, the TRR should be inside of an aluminium shield.

4.4 Temperature Source

The chiller HEC006 from SMC Corporation using water as a coolant was chosen as the temperature source, because it was already available at MI-Partners. This is a limitation to the design, since the cooling capacity when using water is limited to the range of 10 °C to 60 °C, as shown in Figure 5.

In order to calibrate sensors in the calibration range of 10 °C to 50 °C the source's temperature range must be larger than the calibration range, because the thermal capacitance of the system prevents the TRR's temperature of having the same calibration range

Figure 4 – Effectiveness of the aluminium shield in avoiding thermal disturbances

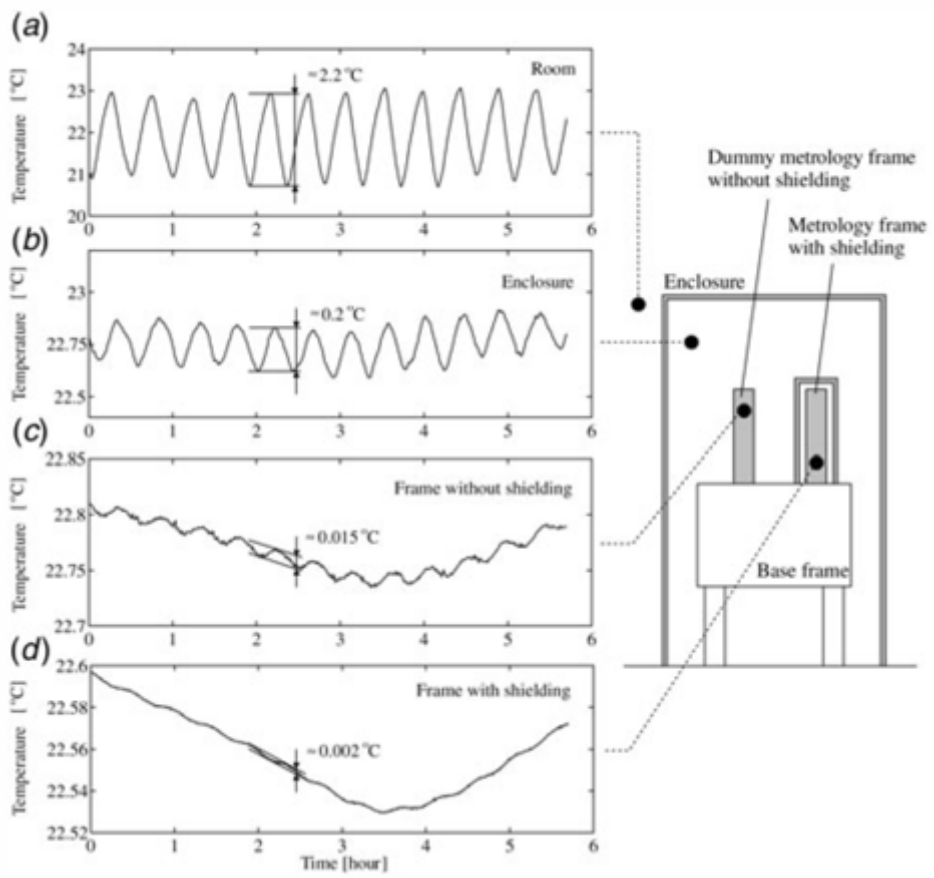

Source: Ruijl (2001)

Figure 5 – Temperature range of different coolants of the chiller HEC006 from SMC

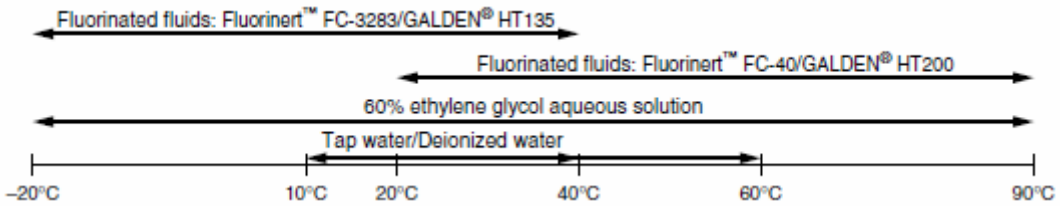

Source: SMC (2019)

of the source. Therefore, the ideal option would be a solution of 60% ethylene glycol whose range is -20 °C to 90 °C.

4.5 Conceptual Design

So far, this chapter has presented reasons for the design choices in order to have a thermal reference region with high temperature homogeneity. This subsection combines all design choices made to create a conceptual design of the calibration tool.

Figure 6 illustrates the cross-section view of the conceptual design of the system. The frame consists of three concentric cylinders. The outside cylinder is the shield, which is made of an aluminum cylinder shell with channels for the water-cooling system. The shield has two main functions. First, it serves as an actuator controlling the temperature of the TRR . Second, it cancels disturbances from the environment. To ensure temperature homogeneity of the TRR, the shield should be isothermal as well. The intermediate cylinder is the insulation (foam) and the inner cylinder is the TRR (aluminum), on which the sensors will be placed .

Figure 6 – Cross-section view of the conceptual design

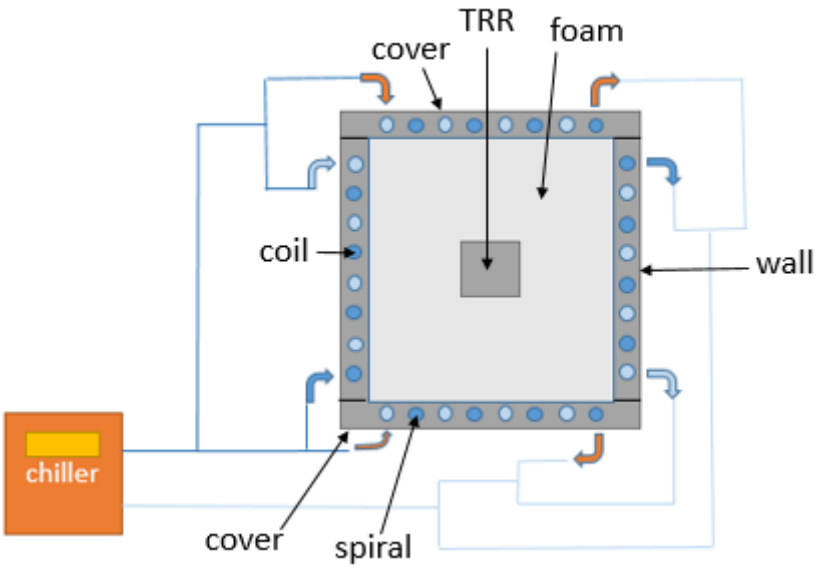

Source: Author

To simplify the description and further explanations the parts of the frame will be referenced as follows:

- wall: shield lateral side.

- coil: channels in the wall.
- cover: shield‘s upper and bottom part.
- spiral: channels in the cover.
- insulation: foam.

As explained, the shield needs to be isothermal to work as an isothermal temperature source for the TRR. However, if the shield is at T_{env} and water is injected at $T_{in} < T_{env}$, into the coil entrance. It is expected that the water will warm up and at the end of the coil the water temperature will be $T_{out} = T_{in} + \triangle T$, it means that there is a temperature gradient in the coil, so the shield is not isothermal. The same occurs in the spiral. The solution for this problem consists of two coils with intercalated channels and opposite water flow directions. This is illustrated in Figure 6 by the different shades of blue. The same principle can be applied in the design of the spiral. This design allows the channels to exchange heat and achieve an average temperature, which results in an isothermal wall and cover. Note that to make the shield isothermal, it is necessary to make the temperature of the wall equal to the temperature of the cover.

In summary, the calibration tool's main operating idea lies in following the heat flow throughout the system. First, the chiller changes the water's temperature in order to perform the calibration at the specified calibration range. Then, the water flows through the channels inside the shield. The shield reduces the TRR sensitivity from thermal disturbances. All the heat that flows from the shield walls is reduced by the foam, whose thickness must be designed such that the TRR can vary its temperature within the calibration range. Finally, the heat that enters the TRR results in an increase in temperature. This temperature will be homogeneous due to the high thermal conductivity of aluminium. Consequently, it is expected that the thermal region has a high temperature homogeneity. The following chapters aim to verify if the design concept is able to achieve the setting requirements and to show the details of the design.

5 Error Analysis

This chapter presents an analysis of the errors related to the calibration of temperature sensors in this calibration tool. The major sources of error were identified, some of them were related to the whole system and others, to invidual sensors differently. For this reason, independent analyses for thermocouples, RTD and NTC were needed. It was possible to solve some of these errors, while for others there were no possible solutions. Finally, relative error, specific for this project, was defined and the relative error for each sensor was evaluated and analyzed.

5.1 Sources of error

To analyze the measurement error, all major sources of error of the calibration system should be identified. It opens the possibility to improve the design by searching for better solutions to reduce error magnitudes or even make them negligible. In this section, the calibration tool's main sources of error are presented and analyzed. In some cases solutions are given.

As mentioned in the Section 3.2, a general comparison calibration set-up requires: measurement equipment, a reference sensor, and a TRR. The data acquisition equipment available at MI-Partners is the digital multimeter (DMM) 34970A from Keysight Technologies, Inc. This data logger has high resolution, accuracy, stability, and it has 4-wire connection configuration, which significantly improves the measurement accuracy of resistance based sensors.

It is possible to divide the sources of error into two types: general and specific. The general sources of error are intrinsic to the system and they affect all sensor types in the same way, while the specific sources of error affect each sensor type differently. In this case, it is necessary to analyze each sensor separately.

5.1.1 General Source of Errors

Conduction via cables

Ruijl (2001) shows that the surrounding air has a large influence on temperature measurements. Copper wires connected to sensors and exposed to air, are cooled or heated by convection. Therefore, the sensors are also cooled or heated by conduction because of the high conductivity of the wires. As a result of this heat transfer process, there is a measurement error. Ruijl (2001) also proposed a solution, which consists of fixing the wire to the body on which the sensor is placed. This makes the wire temperature equal to the sensor temperature, which reduces conduction through the cable, and consequently, reduces surrounding influence. Figure 7 is part of an experimental set-up which shows that the measurement error, due to a incorrect installation of the sensor, is significant. In addition, it has been proven that this solution is effective (RUIJL, 2001)

Figure 7 – Proper installation of the sensor to avoid conduction via cables.

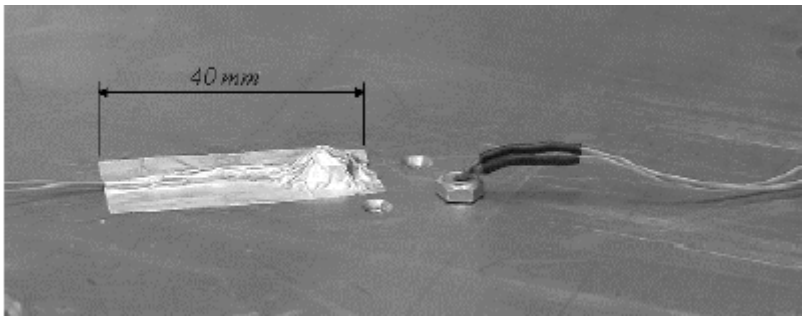

Source: (RUIJL, 2001)

Regarding the correct sensor installation, it is necessary to calculate the length of the wire that needs to be fixed. Thus, the same solution can be applied in this project. It can be done using Equation (23), which was adapted from the equation to conduction and convection in a fin of uniform cross-section (INCROPERA et al., 2007, p. 144). In Equation (23), when $T(x) - T_{air}$ goes to zero for $x = x_{air}$. In means that $T(x_{air}) \simeq T_{air}$. Therefore, the influence of the T_{air} start from $x = x_{air}$ until achieve the sensor in $x = 0$. The conduction through the length of the wire given by x_{air}, must be avoided fixing this length on the TRR's surface.

$$\frac{T(x) - T_{air}}{T(x=0) - T_{air}} = e^{-x\sqrt{\frac{h\pi d_{insulation}}{k\frac{\pi}{4}d^2_{wire}}}} \tag{23}$$

where: $k_{Cu} = 355\ [W/°Cm]$ is the conductivity of the wire; $h = 7\ [W/°Cm^2]$ is an estimation of the convection coefficient of air; and $d_{insulation} = 1\ mm$ is the wire's outside diameter. The results in Figure 8 shows that to make this error negligible, wire with the diameter 0,1 mm 0,3 mm and 0.5 mm should have a length fixed to the frame, equal to 50 mm, 150 mm, 250 mm respectively.

Figure 8 – Length of wire that should be fixed to avoid conduction via cables.

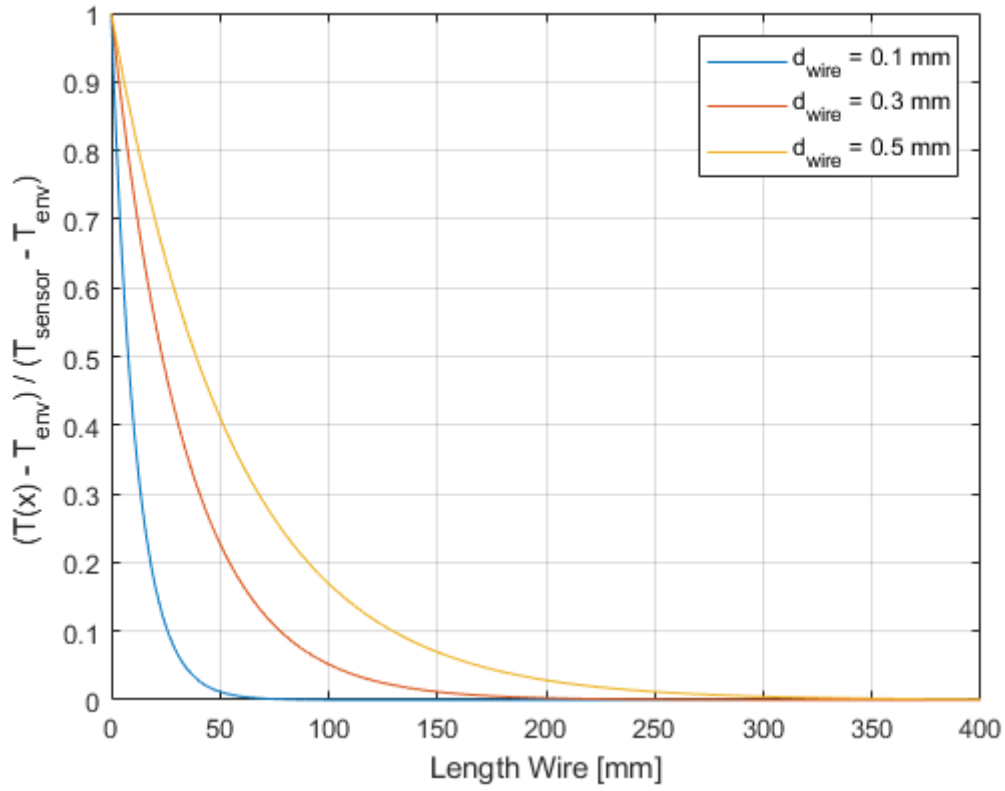

Source: Author

Positioning Error

A difference in the location of the sensors produces a difference in the temperature of the measurand, because of the temperature gradient in the TRR. For this reason, it is necessary to understand the temperature gradient of the TRR. In this sense, the analysis can be tackled considering the heat flow from the cover and the wall independent from each other.

From the perspective of the heat flowing from the cover, the TRR is a plane wall. Hence, the temperature distribution is linear through the cylinder in the vertical direction

(INCROPERA et al., 2007, p 98). It means that if the sensors are positioned at the same height of the TRR they will measure the same temperature. This can easily be done, for example, by positioning the sensors on the top surface. However, from the perspective of the heat flowing from the wall, the TRR is a cylindrical wall. Hence, the temperature has a logarithmic dependence to the radius of the TRR (INCROPERA et al., 2007, p 117). It means that if the sensors are not positioned in the same radius, they will measure different temperatures. This temperature difference will be called the positioning error.

As discussed previously, the main aspect of the calibration tool design is to develop an TRR isothermal enough to consider the positioning error negligible. Note that decreasing the radial temperature gradient is equivalent to reducing the positioning error. It was defined that the positioning error is negligible if the temperature homogeneity is less than 0,5 mK/mm for the TRR, see Chapter 2. Indeed, this is a fundamental aspect of this project, such that Chapter 6 is completely dedicated to the analysis of the positioning error in order to make this error negligible.

5.1.2 Specific Sources of Error

Self-Heating Error (SHE)

The self–heating error is an inherent characteristic of resistor-based sensors, because of the heat dissipated by the Joule effect. The power P $[W]$ dissipated by a resistance R $[\Omega]$ due to a current i $[A]$ is given by

$$P = Ri^2 \tag{24}$$

And the heat energy Q $[J]$ due to a difference in temperature $\triangle T$ $[^\circ C]$ is given by

$$\triangle Q = mc_p \triangle T \tag{25}$$

Thus, self-heating error ε_{sh} can be evaluated through the combination of 24 and 25, as following:

$$\begin{aligned} P &= Ri^2 \\ \frac{\triangle Q}{\triangle t} &= Ri^2 \\ \frac{mc_p \triangle T}{\triangle t} &= Ri^2 \end{aligned}$$

where $\triangle T$ is the increasing temperature of the resistance based sensor due to a current i passing during a time interval $\triangle t$. Therefore, the temperature difference is the error due to self-heating $\triangle T = \varepsilon_{sh}$, expressed by

$$\varepsilon_{sh} = \frac{Ri^2 \triangle t}{mc_p} \tag{26}$$

where m is the sensor's mass; c_p is the specific heat capacity of the sensor and $\triangle t$ is the current pulse time applied to the sensor. As specified in (KEYSIGHT, 2018), The DMM works with 10 Power Line Cycle (PLC), so the $\triangle t = 2\ s$ for all sensors. The current changes depending on the work range of the sensor and is given in Keysight (2018). The mass for all sensors was estimated as $m = 1.10^{-5}\ [kg]$ based on (LAKESHORE, 2019?). For RTD, a platinum sensor was used, whose specific heat capacity is $c_{p_{platinum}} = 130\ [J/KgK]$ (TOOLBOX, 2003b). For NTC was used $c_{p_{epoxy}} = 1000\ [J/KgK]$ (TOOLBOX, 2003a) due to the packing of epoxy.

Digital Multimeter Measurement Error (DMME)

DMME (ε_m) includes all switching errors and includes ITS-90 conversion errors as well. The equation to determine DMME is specified as the percent of reading plus the percent of work range (KEYSIGHT, 2018):

$$\varepsilon_m = \pm(\%\text{ of reading x measured value} + \%\text{ of range x work range}) \tag{27}$$

where, percent of reading, percent of range and work range are given by Keysight (2018). The percent of reading and the percent of range depends on the calibration cycle. In this project was used the 24-hours specification.

ε_m has the unit of the physical quantity being measured. It is resistance [Ω] for resistance based sensors, and voltage $[V]$ for thermocouples. Therefore, DMME must be divided by the sensitivity of the sensor in order to obtain (ε_m) in temperature units.

5.2 Evaluating Errors

The sensors used to evaluate the errors are:

- Thermocouple type J,[1] due to its high sensitivity of 55 uV/°C compared with others thermocouples.
- Pt 100 and Pt1000[2] whose sensitivity is 0,4 Ω/°C and Pt1000 4 Ω/°C, respectively.
- NTC - Accurate series: NTC 10K, NTC 50K, NTC 100K[3].

The sensitivity of the NTCs has an exponential relation between resistance and temperature. The sensitivity for each temperature can be evaluated by $\frac{R_t \alpha}{100}$, where α and R_t are given in (AVX, 2019).

Table 2 – Errors for NTC: 10KΩ, 50KΩ and 100KΩ

Temp.$[°C]$	NTC					
	10k		50k		100k	
	$\pm\varepsilon_m[mK]$	$\varepsilon_{sh}[mK]$	$\pm\varepsilon_m[mK]$	$\varepsilon_{sh}[mK]$	$\pm\varepsilon_m[mK]$	$\varepsilon_{sh}[mK]$
10	0.9066	0.0406	0.5037	0.2047	1.3396	0.1044
20	1.2876	0.0252	0.5954	0.1262	2.0486	0.0635
30	1.8830	0.0160	0.7297	0.0797	3.1865	0.0396
40	2.7950	0.0104	0.9297	0.0515	4.9872	0.0253
50	4.1756	0.0070	1.2237	0.0340	7.7829	0.0165

Source: Author

The NTC sensitivity increases with increasing sensor resistance. That is why the ε_m of the NTC 50K is smaller than the ε_m for NTC 10K in Table 2. However, this does not happen for the NTC 100K because the percent of reading for NTC 10K and NTC 50K is 0.0005, while, the percent of reading for NTC 100K is twice as much, i.e., 0.001. On the other hand, the current applied to NTC 100K is half of the current used in the 10K and 50K, which reduces self-heating error.

Table 3 – Errors for Pt100 Pt1000 and Thermocouple type J

Temp.$[°C]$	RTD				Thermocouple
	Pt 100		Pt 1000		Type J
	$\pm\varepsilon_m[mK]$	$\varepsilon_{sh}[mK]$	$\pm\varepsilon_m[mK]$	$\varepsilon_{sh}[mK]$	$\pm\varepsilon_m[mK]$
10	20.1989	15.9966	17.6989	1.5997	64.1922
20	20.3974	16.6073	17.8974	1.6607	64.4747
30	20.5952	17.2161	18.0952	1.7216	64.7595
40	20.7925	17.8231	18.2925	1.7823	65.0464
50	20.9892	18.4283	18.2925	1.8428	65.3360

Source: Author

[1] The values of voltage used to evaluate DMME can be found in (THERMOCOUPLEINFO.COM, 2011)
[2] The values of resistances used to evaluate SHE and DMME can be found in (**??**)
[3] All parameters used in the calculations can be found in (AVX, 2019)

In Table 3 it is clear that the RTD sensors and the thermpocouple sensor have higher errors than the NTC sensors (Table 2). The main reason for this is that the NTCs' sensitivities are considerably higher than those of the RTDs and the thermocouple's sensitivity. In addition, self-heating has a big influence on RTD sensors because of the high work current of these sensors. For example, Pt100 works with 1 mA and Pt1000 with 0.1 mA, whereas the NTC 10K and the NTC 50K work with 10 uA.

5.3 Relative Error Definition

The temperature difference between points on the frame of machines is fundamental to analyze their thermal deformation, as discussed in Chapter 1. In other words, this temperature difference must be measured accurately. Because of this, a specific definition of relative error is developed in this section

Figure 9 – Illustration of relative error definition

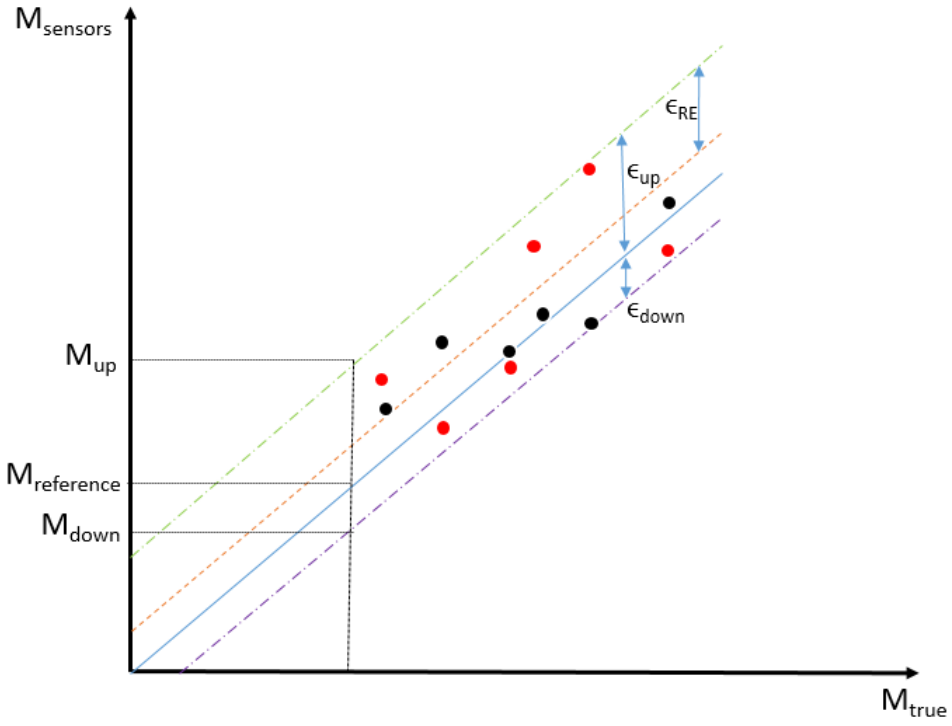

Source: Author

In Figure 9 the X axis represents the true value and the Y axis represents the values measured by the sensors. A measurement system might have several sources of error. The measured quantity value[4] may have increased, decreased or both, due to errors. Sources of

[4] quantity value representing a measurement result.(JCGM, 2008).

error, such as digital measurement equipment can both increase or decrease the measured quantity value with respect to the reference quantity value[5], while other errors can only increase or decrease, as we saw in the case of self-heating in temperature sensors.

To explain the relative error, we will call the sources of error which are able to increase the measured quantity values as ε_{up}, and the sources of error which are able to decrease the measured quantity values as ε_{down}. Then, the measured values due to ε_{up} and ε_{down} are M_{up} and M_{down} respectively. In Figure 9, the blue line represents the reference quantity values, the green and purple lines represent values that are measurable due to ε_{up} and ε_{down}, respectively. The red line is the mean between the green and purple line. Relative error is defined as the distance between the value from ε_{up} or ε_{down} and the mean value of these two values. Thus, mathematically, the relative error can be expressed as $\varepsilon_{RE} = \frac{|\epsilon_{up} - \epsilon_{down}|}{2}$. The relative error is a way to estimate the closeness between the measured values and its mean value.

5.3.1 Relative Error of the Sensors

Previously, the definition of relative error has been developed in a general way. However, in the case of temperature measurements, it is important to note that this definition only makes sense for calibration of temperature sensors of the same type, because ε_{up} and ε_{down} depend on the type of the sensor. For this reason, ε_{sh} and ε_{m} have been evaluated for each sensor type. Finally, after all sources of error have been analyzed and quantified, it is possible to evaluate the relative error.

Making an analogy with the terms used in section 5.3 to define relative error, it is possible to identify that $\varepsilon_{up} = \varepsilon_{sh} + \varepsilon_{m}$ and $\varepsilon_{down} = \varepsilon_{m}$. Thus, the relative error is $\varepsilon_{RE} = \frac{|\varepsilon_{up} - \varepsilon_{down}|}{2}$, which in the case for NTCs and RTDs is $\varepsilon_{RE} = \frac{|2\varepsilon_{m} + \varepsilon_{sh}|}{2}$. For thermocouples there is no ε_{sh}, then the relative error is equal to the ε_{m}.

From Table 4, it is clear that the sensor type NTC has the best results. The relative error of the NTCs are about twenty and sixty times smaller than the relative error of the RTDs and the thermocouple type J respectively. Among the NTCs the 50k presents the smallest relative error. However, it does not achieve the objective of a calibration tool which is able to calibrate temperature sensors with a relative error smaller than 0.5 mK. The absolute error can be determined by summing up the relative error to the reference

[5] quantity value used as a basis for comparison with values of quantities of the same kind.(JCGM, 2008)

Table 4 – Relative error for all sensors analyzed

	ε_{RE} $[mK]$					
Temp.$[°C]$	NTC			RTD		Thermocouple
	10K	50k	100k	Pt 100	Pt 1000	Type J
10	0.9270	0.6061	1.3917	28.1972	18.4987	64.1922
20	1.3002	0.6585	2.0803	28.7010	18.7277	64.4747
30	1.8910	0.7696	3.2063	29.2033	18.9561	64.7595
40	2.8002	0.9555	4.9998	29.7041	19.1837	65.0464
50	4.1791	1.2407	7.7911	30.2033	19.4106	65.3360

Source: Author

sensor accuracy, which in the case of this project is about 1 mK. Thus, the requirement of absolute error smaller than 3 mK is achieved by the NTC 50K sensor.

6 Thermal Reference Region (TRR)

This chapter contains the process and reasoning used to design a thermal reference region with enough temperature homogeneity to consider the positioning error negligible, see subsection 5.1.1. The design process follows the methodology suggested by Ruijl (2011). First of all, the analysis of the system was made via lumped masses modelling. It is essential to understand the behavior of the system, identify the key parameters and make changes quickly in the design. After that Finite Element Method (FEM) analysis was performed via software ANSYS, and both analyses were compared to validate the results.

6.1 Temperature Gradient Modelling

The physics behind this design consists in controlling the heat flow into the thermal reference region. In this sense, the source of heat can be used to divide the system in two subsystems. (1) the wall-subsystem, which considers the heat flow from the water of the coil (or wall) and (2) the cover-subsystem, which considers the heat flow from the water of the spiral (or cover). The approach used to design the TRR only considers the heat flow from the wall-subsystem and considers the heat from the cover-subsystem negligible. This simplifies the design, since controlling one source of heat flow is easier than controlling two sources. Moreover, it facilitates the overall understanding of the behaviour of the system, because if there are two heat sources it is difficult to identify the one that produces a certain effect. Thus, the first model considers only the wall-subsystem. Therefore, the water temperature T_{water} in Figure 10 refers to the water of the coil.

In order to proceed with the modelling, the dimensions of the thermal reference region, which is an aluminum cylinder (section 4.5), need to be defined. This cylinder needs to have sufficient space to install temperature sensors (including the wire length fixed to the cylinder to avoid conduction via cables). On the other hand, the finished design cannot be too large in order to avoid having a big thermal capacitance and having a big calibration tool. Therefore, the dimensions chosen were 30 mm for the radius and 60 mm for the height. The same height was used for the foam in the modelling.

Due to the temperature gradient in the thermal reference region, a difference in the location of the sensors produces a difference in the temperature (positioning error). Thus,

Figure 10 – LMM to analyze the positioning error due to 1 mm distance between two points in the radial direction in the middle of the TRR

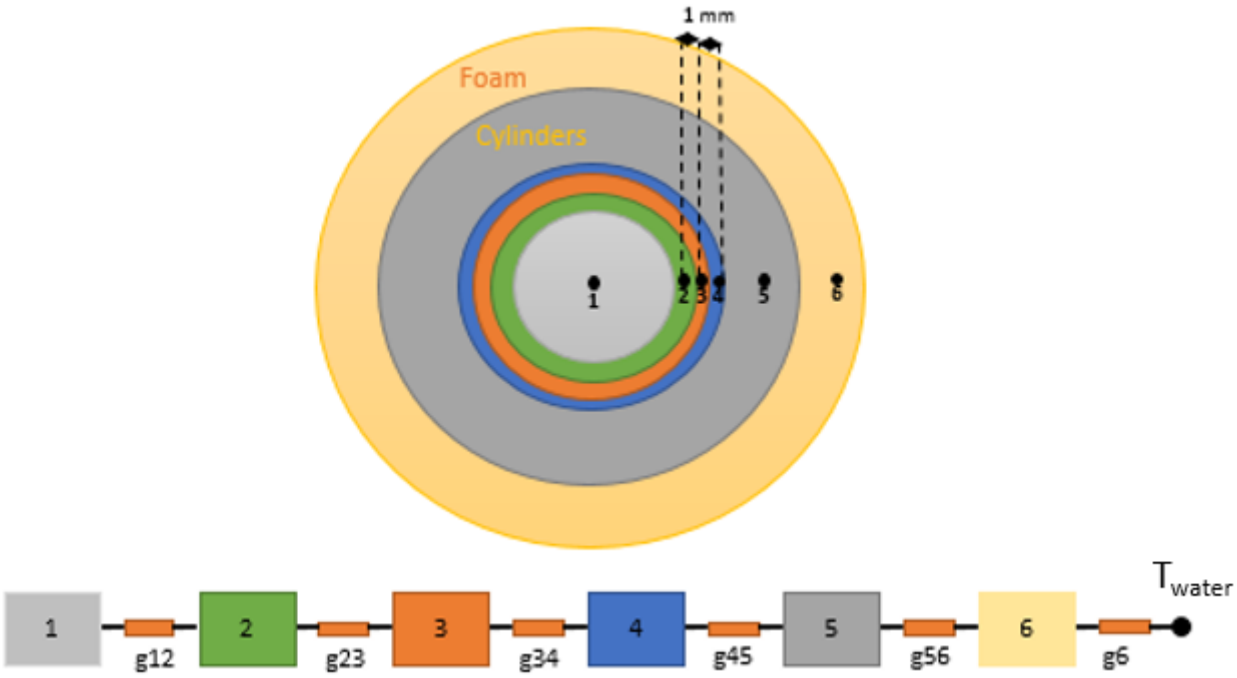

Source: Author

measuring the gradient between two points is the same as measuring the positioning error due to the distance between these points. This idea was used to analyze the positioning error due to 1 mm distance between two points in the middle of the cylinder. Therefore, in the model the TRR has been divided into five cylinders, which can be seen in top view in Figure 10. The masses 2, 3 and 4 in the middle of the cylinder's radius have 1 mm thickness in order to obtain the positioning error due to 1 mm difference in the location by evaluating the absolute temperature difference between these points, such as $|T_2 - T_3|$ and $|T_3 - T_4|$.

The design process to obtain a negligible positioning error consists of increasing the foam's radius until the TRR achieves temperature homogeneity smaller than 0.5 mK/mm, according to Chapter 2. It is important to mention that this process takes just a few minutes using LMM.

The temperature input used in all modelling and simulations is one period of 24 hours of a sinusoidal wave which starts at 20 °C, and whose the maximum and minimum value are 60 °C and 10 °C respectively. This input corresponds to the range of the water-cooled chiller discussed in the Section 4.4.

Figure 11 shows the results of $|T_2 - T_3|$ and $|T_3 - T_4|$ for foam's radius of 90 mm. The first peak of magnitude corresponds to the transient response. It means that the values of interest are in the second peak (stationary response). Thus, analyzing the second peak for $|T_2 - T_3|$ and $|T_3 - T_4|$, it is reasonable to conclude that the temperature homogeneity in the middle of the TRR's radius is around 0.065 mK/mm, which is almost ten times better than required value of 0.5 mK/mm. In addition, as the sensors are placed closer to the cylinder's core, the positioning error decreases, as we can see $|T_2 - T_3| < |T_3 - T_4|$.

Figure 11 – Results of the positioning error due to 1 mm of distance between two points in the middle of the TRR

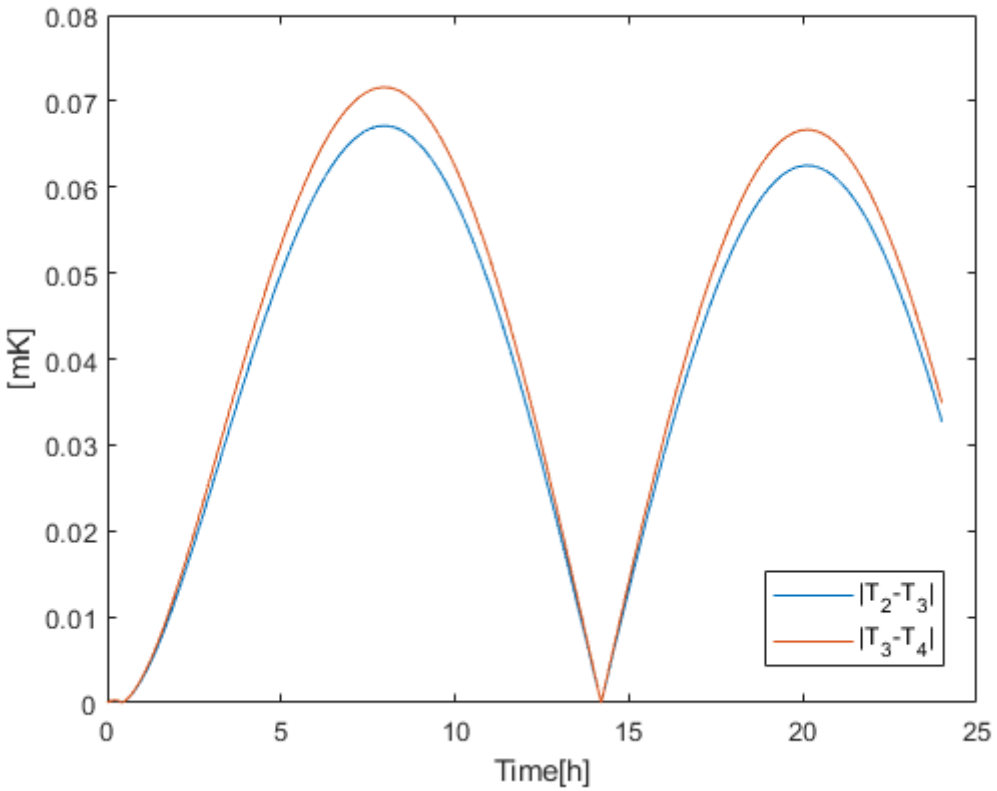

Source: Author

6.2 Complete Modelling

In order to include the heat flow from the cover-subsystem in the analysis of the temperature homogeneity of the TRR, a complete model, including both subsystems was made, see Figure 12. Note that to perform the simulation some parameters needed to be assigned, because the model was still missing a lot of information about the complete system. The heat conductivities from the environment g_{env-c} and g_{env-w} were considered

zero. This means that there is no heat flowing into the system from the environment. For the g_{spiral} and the g_{coil} a value of 20 W/K has been chosen. This value allows for good coupling between the cover's temperature, the wall's temperature and water's temperature in order to make the shield isothermal (Figure 13). Moreover, the shield thickness was defined as 25 mm in order to evaluate the mass of each part.

Figure 12 – Complete Lumped Mass Model of the system

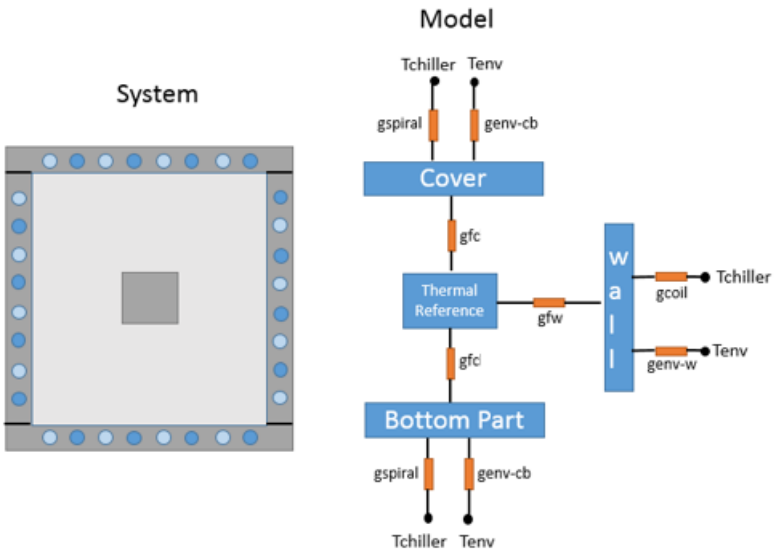

Source: Author

In order to maintain the high temperature homogeneity of the TRR, obtained by only considering heat flow from the wall-subsystem. The next step in this design process consisted of making the heat flow from the cover-subsystem as small as possible.

Figure 13 illustrates the process of determining the foam thickness. The contribution of the heat flow from the cover in the TRR's temperature was analyzed by comparison. First, the TRR's temperature was evaluated for $g_{fc} = 0$ which means there was no heat flow from the cover, and consequently, the cover-subsystem did not influence the TRR's temperature. Secondly, the TRR's temperature was evaluated for increasing values of foam thickness, such as 30, 60, 90 and 120 mm, see Figure 13. Thus, comparing the TRR's temperature (for example, the maximum temperature) when $g_{fc} = 0$ to the TRR's temperature for different foam thicknesses ($g_{fc} \neq 0$) it is possible to analyze the influence of the heat flow from cover-subsystem. It is important to mention that for each 30 mm of foam thickness added, the height and mass of the whole system increase 60 mm and about 3.3 kg.

Figure 13 – Process to determine the foam thickness between the cover and the thermal reference region

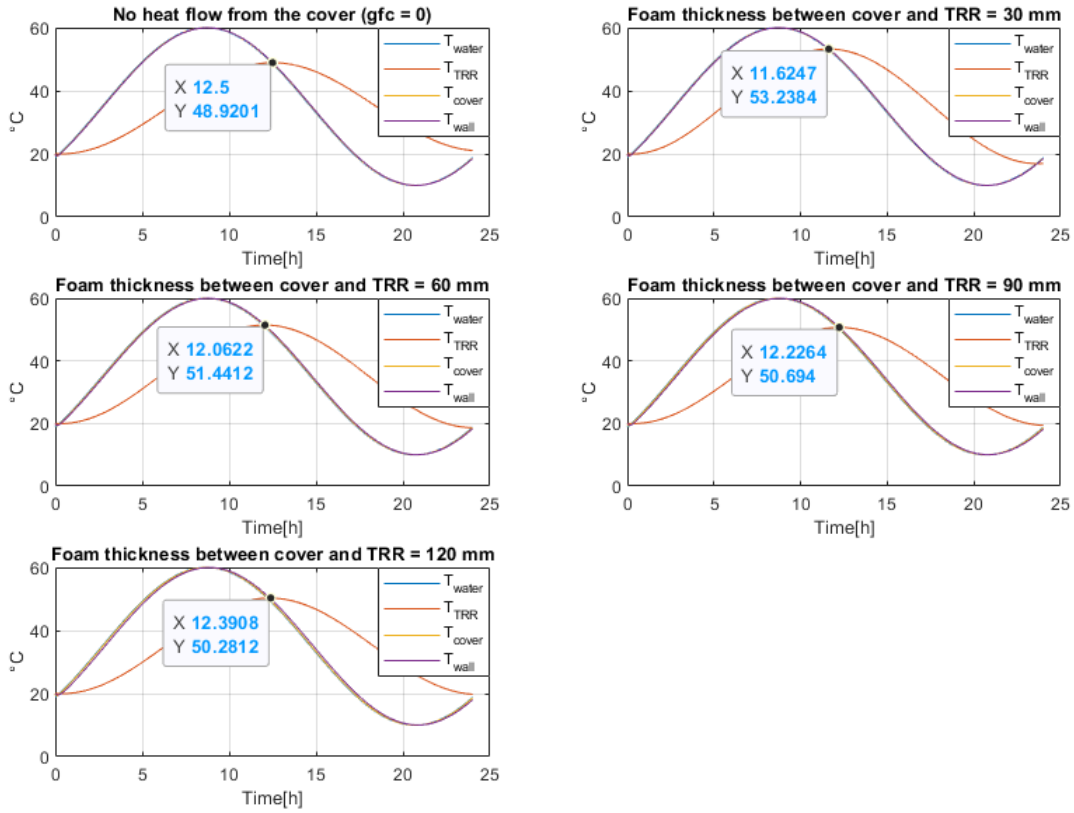

Source: Author

Analyzing Figure 13, we see that even when the foam's thickness is only 30 mm between the cover and the TRR, the influence of the heat flow from the cover on TRR's temperature is about only 4.33 $°C$. This because the TRR is mainly influenced by the wall-subsystem since much more heat flow comes from this subsystem due to the geometry of the calibration tool. This comparison was made as $T_{th=0} - T_{th=30} = 53.23\ °C - 48.92\ °C = 4.33\ °C$. Making the same comparison for the other values of thickness, it is possible to see that for 60 mm the influence is about 2.54 $°C$, for 90 mm the influence is about 1.79 $°C$ and for 120 mm the influence is about 1.37 $°C$. The influence of the cover-subsystem decreased only 0.42 $°C$ from 90 mm to 120 mm of thickness. This reduction is not worth the system's gain of weight and height. For this reason, 90 mm of thickness of the foam between the cover and the TRR was chosen.

6.3 Finite Element Method

With a consistent design of the foam, it was possible go further in the analysis of the temperature homogeneity. With this proposal, a FEM was done using ANSYS' Transient Thermal Tool.

Figure 14 shows the cross-section of the model with the heat flow in the moment at which it is highest. In this way the worst case for the temperature homogeneity is analyzed. Note the difference in the quantity of light blue vectors of heat flow from the cover and wall. It can be seen that the wall-subsystem has a stronger influence on the thermal reference region's temperature, as the reasoning applied in the section 6.2 suggested. The heat flow from the shield into the thermal reference region creates an "entrance region" at the cylinder's corner with high non-homogeneity in temperature.

Based on the heat flow inside the cylinder, the temperature homogeneity increases in the direction of the TRR's core as expected because of the frame symmetry. This supports the results of section 6.1 (Figure 11) but, more than this, it is also possible to observe that the same occurs in the vertical direction (heat flow from the cover). Thus, this suggests that the best location to install the sensors is inside the thermal region as near as possible the cylinder's core.

Figure 14 – Cross-section view of the heat flow in the foam and TRR

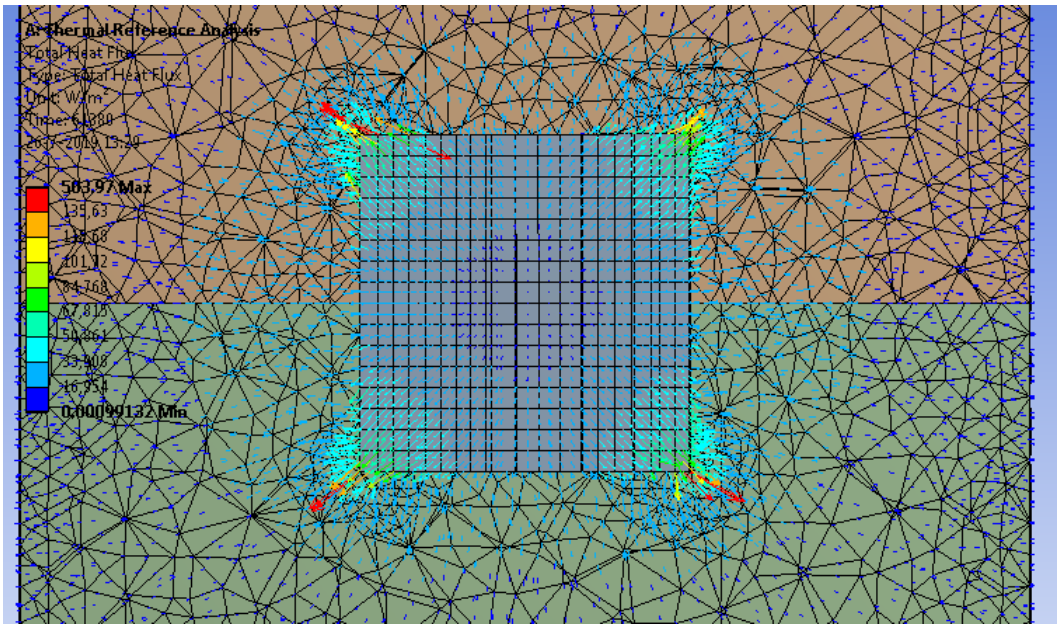

Source: Author

Figure 15 also shows the temperature distribution at the instant of highest heat flow. In addition, it shows how the temperature gradient was evaluated. The temperature of the middle, vertical edge and horizontal edge were measured and the difference of the temperature between each edge and the middle was divided by the distance between these points (30 mm). The results for the $\Delta T_{vertical} = \Delta T_{horizontal} = 0.066$ [mK/mm]. Note that the FE analysis evaluates the gradient in the whole radius, whereas the LM only considers two points separated by 1 mm. Despite the difference in the approach, both analyses show comparable results. Moreover, it indicates that the LMM approach is effective to verify the thermal gradient between two points (1mm apart) in the middle of the TRR's radius. At the bottom of Figure 15, there is the graph of the thermal reference region's temperature which shows the calibration range of 16.5 $°C$ till 53.8 $°C$. This range is comparable to the range of 19.4 $°C$ to 50.7 $°C$ obtained from LMM. This range can be seen in the temperature of the TRR when the thickness of the foam is 90 mm. This similarity is one more argument to validate both the modelling and the simulation.

Figure 15 – Temperature distribution and TRR's temperature during the simulation

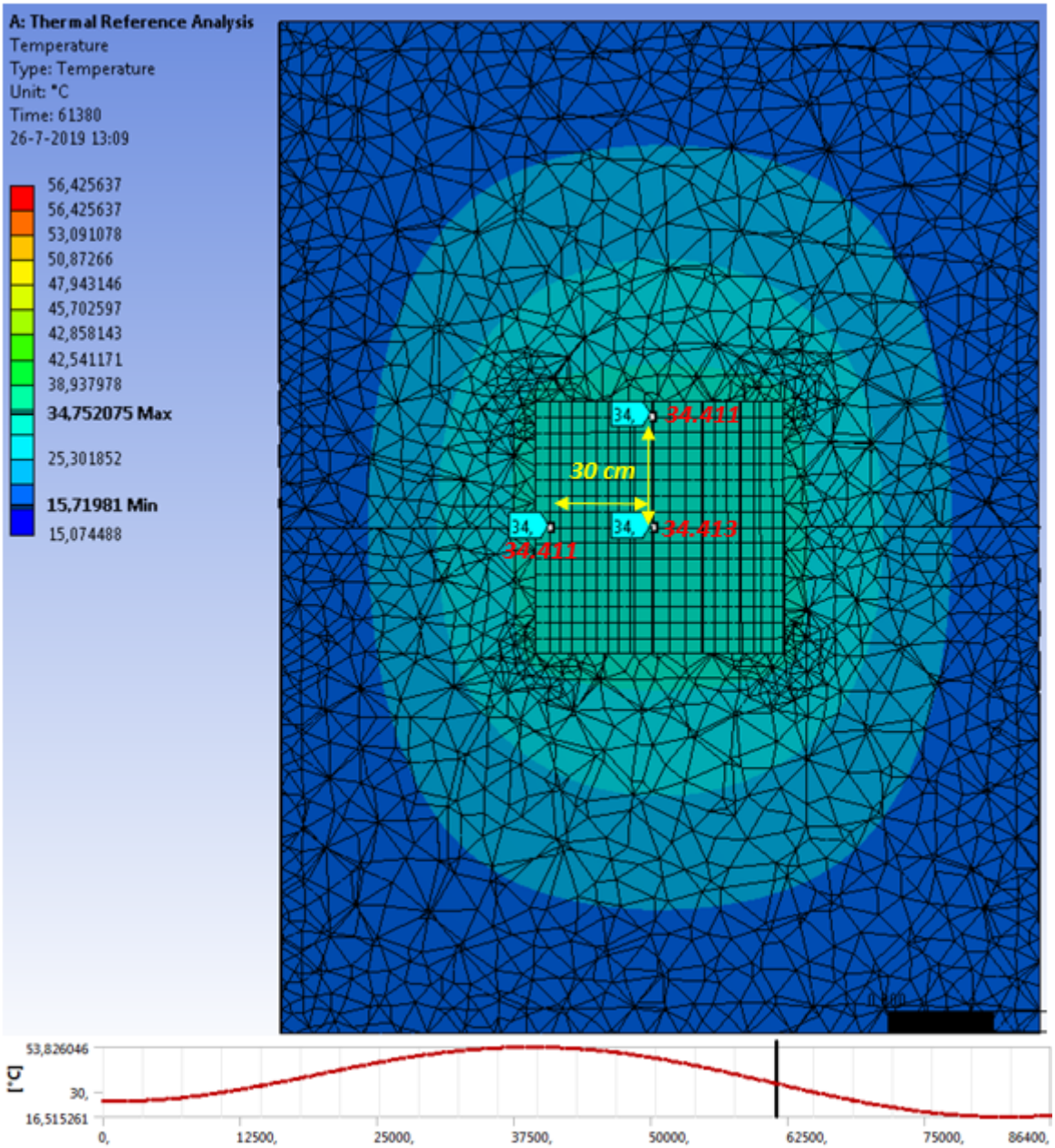

Source: Author

7 Design Optimization

Design optimization is about enhancing the performance of the shield, which works as an isothermal temperature ($T_{wall} = T_{coil}$) source for TRR and protects the TRR from thermal disturbances. This is done in this chapter by making the cover and wall subsystems with the same dynamic behaviour. This includes the definition of the parameters of the spiral and coil channels, as well as the system's hydraulic design. In addition, regarding the shielding efficiency, the comparison between the laminar and turbulent flow has been made.

7.1 Design of the Channels

So far, in all analyses the temperature of the wall and the cover have been considered the same. Now, it is necessary to ensure that the wall and the cover temperatures are equal. Both the wall-subsystem and the cover-subsystem have the same physics, which consist of water changing the temperature of an aluminum body by convection heat transfer. This can be easily modelled, as illustrated in Figure 16.

Figure 16 – Modeling water channel and aluminum mass

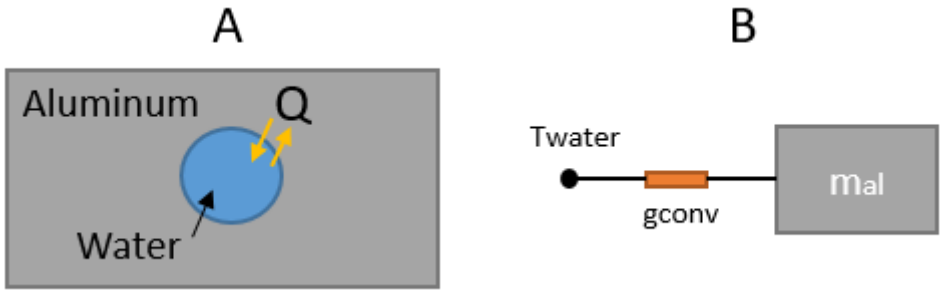

Source: Author

The transfer function for this system is:

$$H(s) = \frac{T_{m_{Al}}}{T_{water}} = \frac{1}{\frac{m_{Al}c_{pAl}}{g_{conv}}s + 1} \tag{28}$$

where, m_{Al} is the mass of the aluminum body, c_{pAl} is the specific heat capacity of aluminum, and g_{conv} is the convection heat conductivity of the water in the channel.

As a first order system, the dynamic behaviour of the system is described by the time constant. Therefore, for both subsystems to have the same temperature, they must

have the same dynamic behaviour ($\tau_{wall} = \tau_{cover}$), where τ_{cover} and τ_{wall} are the time constants of the cover-subsystem and the wall-subsystem, respectively.

From Equation 28 the time constant is identified as

$$\tau = \frac{m_{Al}c_{pAl}}{g_{conv}} = \frac{m_{Al}c_{pAl}}{\overline{h}A_s} \tag{29}$$

where A_s is the wetted surface area of the channel.

The $\overline{h}$ is defined as:

$$\overline{h} = \frac{\rho c_p \phi}{A_s}\left(1 - e^{-\frac{N_u k A_s}{d\rho c_p \phi}}\right) \tag{30}$$

for the development of this expression see Appendix A.

Adding 30 into Equation 29, we obtain

$$\tau = \frac{m_{Al}c_{pAl}}{\rho c_p \phi}\left(1 - e^{-\frac{N_u k_{Al} A_s}{d\rho c_p \phi}}\right)^{-1} \tag{31}$$

where ρ $[kg/m^3]$ is the density of water, c_p $[J/Kg°C]$ is the specific heat of water, $\phi[m^3/s]$ is the flow of water, d $[m]$ is the diameter of the pipe, k_{Al} $[W/m.°C]$ is the thermal conductivity of aluminum and N_u is the Nusselt number.

Note that in spite of these many parameter, τ is essentially a function ϕ, d and channel's length L, because $m_{Al},\ c_p,\ c_{p_{Al}},\ k_{Al},\ \rho,$ and Nu for laminar flow are constants. The superficial area is given by $A_s = \pi dL$, which is a function of d and L, where L is the length of the channel. The Nu for turbulent flow (see Equation 13) depends on the flow, since Pr is constant for a determined temperature and the friction factor (see Equation 10) depends on the flow. Therefore, the time constant can be tackled as $\tau_{wall}(d_{coil}, L_{coil}, \phi_{coil})$ for the coil-subsystem and $\tau_{cover}(d_{spiral}, L_{spiral}, \phi_{spiral})$ for the cover-subsystem. Consequently, the time constant has two equations, one for laminar flow and another for turbulent flow.

The length and the diameter were estimated in order to plot $\tau_{wall}(\phi_{coil})$ and $\tau_{cover}(\phi_{spiral})$ in the same graph. After this, the length and diameter for each channel were adjusted until there were equal values for the time constants ($\tau_{wall} = \tau_{cover}$). As this configuration was found, the spiral and coil's lengths and diameters were defined. Figure 17 illustrates the final result of $L_{coil} = 2.6$ m , $d_{coil} = 5$ mm , $L_{spiral} = 0.71$ m and $d_{spiral} = 5$ mm. These lengths are for one coil and one spiral. Due to the fact that the Nu number is not defined in the range $2300 < Re < 3000$, there is a gap between the laminar flow and turbulent flow in Figure 17.

Since it is known that there are values of ϕ_{coil} and ϕ_{spiral} that result in $\tau_{wall} = \tau_{cover}$, it was necessary to identify these flows. This was done by solving Equation 32 using

Figure 17 – $\tau_{wall}(\phi_{coil})$, $\tau_{cover}(\phi_{spiral})$ and regions where $\tau_{wall} = \tau_{cover}$

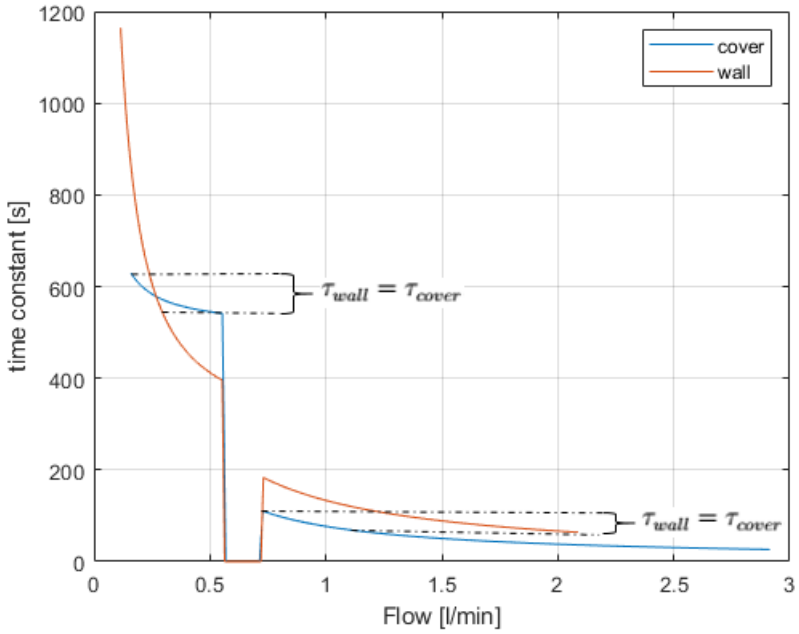

Source: Author

MATLAB's Symbolic Tool for the laminar and turbulent flows. Some of the result values can be seen in Table 5.

$$\tau_{wall}(\phi_{coil}) = \tau_{cover}(\phi_{spiral}) \tag{32}$$

Table 5 – Some examples of flow values which result in the same dynamic behavior for both subsystems

Laminar					Turbulent				
Flow $[l/min]$			$\overline{h}$ $[W/Km^2]$		*Flow* $[l/min]$			$\overline{h}$ $[W/Km^2]$	
ϕ_{spiral}	ϕ_{coil}	ϕ_{sys}	spiral	coil	ϕ_{spiral}	ϕ_{coil}	ϕ_{sys}	spiral	coil
0.3350	0.2786	1.23	397	203	0.7283	1.2089	3.87	2033	1033
0.4079	0.2866	1.39	405	203	0.7866	1.3245	4.22	2228	1131
0.4224	0.2879	1.42	406	208	0.8448	1.4383	4.57	2420	1229
0.4515	0.2903	1.48	408	208	0.8885	1.5226	4.82	2562	1301
0.4952	0.2934	1.58	411	208	0.9905	1.7166	5.41	2888	1470
0.5244	0.2952	1.64	412	208	1.0925	1.9072	6.00	3208	1630

Source: Author

The same table shows the system flow which is the total flow delivered from the water pump to the system. It was evaluated by summing up the flows that pass through the spiral and the coil channels, such as $\phi_{sys} = 2(\phi_{spiral} + \phi_{coil})$. This equation can be easily understood by seeing Figure 18. Table 5 also presents the average heat transfer coefficient ($\overline{h}$) of the water flow in the coil and the spiral. The $\overline{h}$ was evaluated using Equation 30. It will be necessary in the analysis of the dynamic behaviour of the system.

7.2 Hydraulic Design

The hydraulic design has two main goals. One is to analyze the system pressure drop with the purpose of identifing the actual flow of the system. Another is to calculate resistance which needs to be added into the hydraulic system in order to obtain the correct flow distribution presented in Table 5, since those flows result in the coil and the wall subsystems with the same dynamic behavior.

The hydraulic system depicted in Figure 18 is derived from the design concept illustrated in Figure 6. It shows a scheme of the hydraulic system and the circuit analogy with the resistances of each fitting. Only half of the circuit is illustrated due to the symmetry of the system. For the same reason the names of the fittings were written only once. In Figure 18, R_1, R_2, R_3 and R_4 are the resistances of pipe 1, pipe 2, pipe 3 and pipe 4, respectively. R_s and R_c are the resistances of the spiral and coil, respectively. R_K is the resistance of the *Knees*, which is present in the entrance and exit of the spiral and the coil. R_{tsn} is the resistance of the *Tee* fitting where the flow enters for the main pipe and splits. The subscript n refers to the number of the main pipe. R_{tjn} is the resistance of the *Tee* fitting where the two flows join and leave through the main pipe. Again, the subscript n refers to the number of the main pipe.

The resistance Rx corresponds to the resistance which needs to be determined and added to the system to produce the flow that makes the wall-subsystem and cover-subsystem having same time constant (Table 5).

Based on the definition of the loss coefficient (K_l) given by White (2009, p. 389), we will define pressure drop as:

$$\Delta P = K_l C \phi^2 \tag{33}$$

where $C = \frac{8\rho}{\pi^2 d^4}$. Making an analogy with electrical circuits, the pressure drop can be associated with the voltage, the flow squared with the current, and the resistance can be identified in Equation 33 by $R = K_l C$.

In order to analyze the system pressure drop all resistances of the system need to be evaluated. In the following calculations, the length and the diameter of all pipes were chosen to be 1 m and 6 mm, respectively, except for the coil and spiral, whose diameter and length were evaluated in Section 7.1.

Figure 18 – Scheme of the hydraulic system and of the circuit analogy

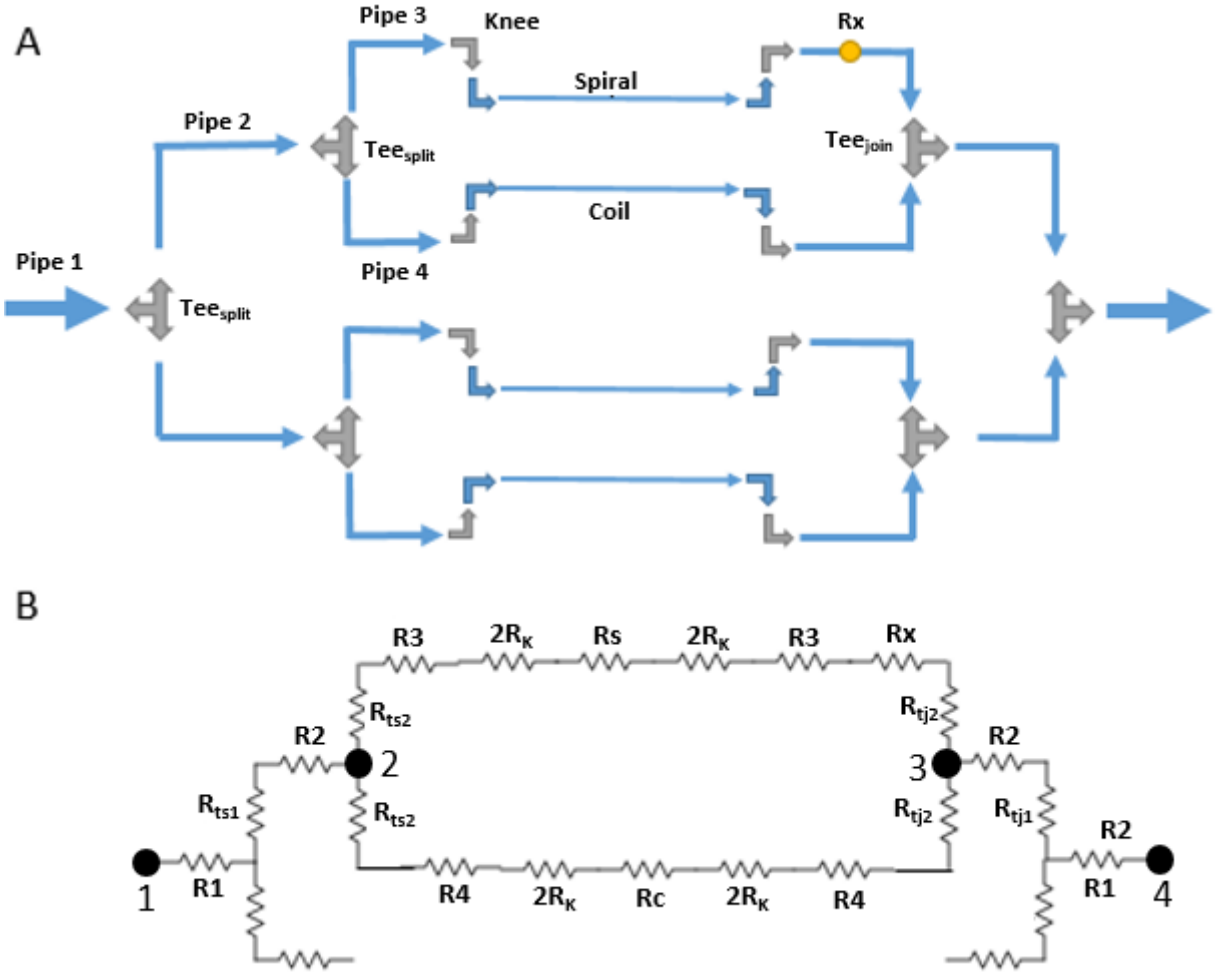

Source: Author

The loss coefficient due to friction is

$$K_l = \frac{fL}{D_h} \tag{34}$$

where f is the friction factor, which was calculated from Equation 9 for the laminar flow and from Equation 10 for the turbulent flow, and D_h is the hydraulic diameter (see Equation 6), which depends on the pipe geometry. We have been considering circular pipes. In this case, the hydraulic diameter is equal to the pipe diameter.

The loss coefficient used for Knee and Tee come from (DUBBEL, 1994) and (JONG, 2002) respectively. They are:

- $K_{Knee} = 1.13$ for smooth pipe.
- $K_{Tee_{split}} = 0.9175$ when the flow enters the main pipe.
- $K_{Tee_{join}} = 0.64$ when two flows leave through the main pipe.

Having defined all loss coefficients, it is possible to evaluate all resistances of the system (see Figure 18).

With these resistances an equation to calculate resistance Rx can be determined. This can be done because the pressure drop between points 2 and 3 are equal. Hence, the pressure drop of the flow which passes in the spiral ($\Delta P_{spiralway}$) is equal to the pressure drop of the flow which passes in the coil ($\Delta P_{coilway}$).

$$\begin{aligned}
\Delta P_{spiralway} &= \Delta P_{coilway} \\
R_{spiralway}\phi^2_{spiral} &= R_{coilway}\phi^2_{coil} \\
\left(R_{ts2} + 2R_3 + 4R_k + R_s + R_x + R_{tj2}\right)\phi^2_{spiral} &= \left(R_{ts2} + 2R_4 + 4R_k + R_c + R_{tj2}\right)\phi^2_{coil}
\end{aligned}$$

Thus, the resistance Rx is given by:

$$R_x = \frac{\phi^2_{coil}}{\phi^2_{spiral}}\left(R_{ts2} + 2R_3 + 4R_k + R_c + R_{tj2}\right) - \left(R_{ts2} + 2R_4 + 4R_k + R_s + R_x + R_{tj2}\right) \tag{35}$$

A simple and versatile solution to add Rx in the system is to insert a narrow pipe as a resistance. The length of the pipe is calculated from (34), which gives

$$l_x = R_x \frac{d_x}{f_x C_x} \tag{36}$$

To solve this equation for l_x the diameter must be defined. In order to make l_x as short as possible a narrow pipe with $d_x = 3$ mm was chosen.

At this point all resistances are known. Hence, it is possible to calculate the equivalent resistance of the system (R_{eq}), which is the equivalent resistance between points 1 and 4 (see Figure 18), in order to determine the total pressure drop of the system as

$$\Delta P_{total} = R_{eq}\phi^2_{sys} \tag{37}$$

Figure 19 – Chiller's pump capacity vs pressure drop of the system for the laminar and turbulent flows

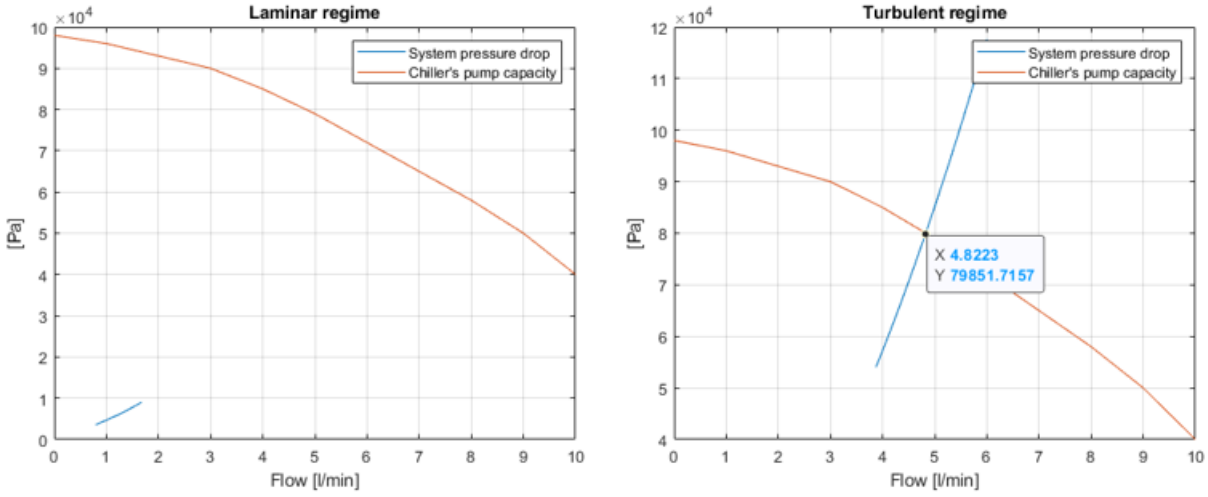

Source: Author

On the one hand, it is clear that for the laminar regime, a less powerful pump must be used, since there is no intersection between the pump capacity curve and the system pressure drop curve. This intersection is termed as pump operation point. On the other hand, in the turbulent regime, the flow is considerably higher, and consequently, the pressure drop of the system as well. As a result, the pump operation point is identified. This point defines the discharge of the pump. In other words, the system flow can be determined, and it is 4.82 l/min. In addition, knowing the flows the value of lx also is determined. It is lx = 743 mm.

7.3 Analysis of the system in the laminar and turbulent flows

In the previous subsection, the system flow of the turbulent region was identified. Looking for this value in Table 5, it is possible to identify the corresponding average convection coefficient for the coil $\overline{h}_{coil} = 621\ [w/m^2.K]$ and for the spiral $\overline{h}_{spiral} = 2083\ [w/m^2.K]$. The same cannot be done for the laminar flow, since there is no operation point when using the existing pump. However, with the propose of analyzing the laminar flow the $\overline{h}_{coil} = 208\ [w/m^2.K]$ and $\overline{h}_{spiral} = 408\ [w/m^2.K]$ which correspond to $\phi_{sys} = 1.48\ [l/min]$ in Table 5 were chosen to perform the analysis. It does not make sense to consider the laminar flow considering the available pump. Nevertheless, the aim of this

section is to compare the dynamic behaviour of the system in the turbulent and laminar regimes. This way, a deeper understanding of the system can be obtained from this project.

With these values, the parameters, g_{spiral} and g_{coil}, of the complete LMM model (see Figure 12) can be evaluated. Moreover, the g_{env-c} and g_{env-w} were evaluated by considering the HTC of the surrounding air to be 7 $[W/m^2.K]$. Finally, these parameters were used in the complete lumped-mass model (see Figure 12). The results for laminar and turbulent flows are shown in Figure 20 and Figure 21 respectively.

Figure 20 – Frequency and time domain analyses for laminar flow

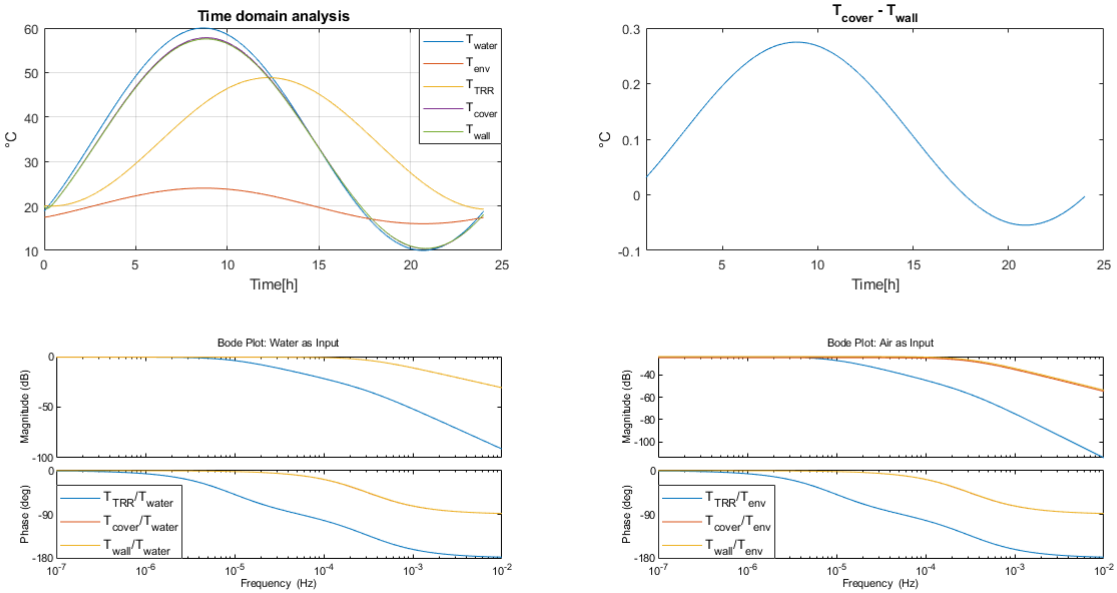

Source: Author

Figure 21 – Frequency and time domain analysis for turbulent flow

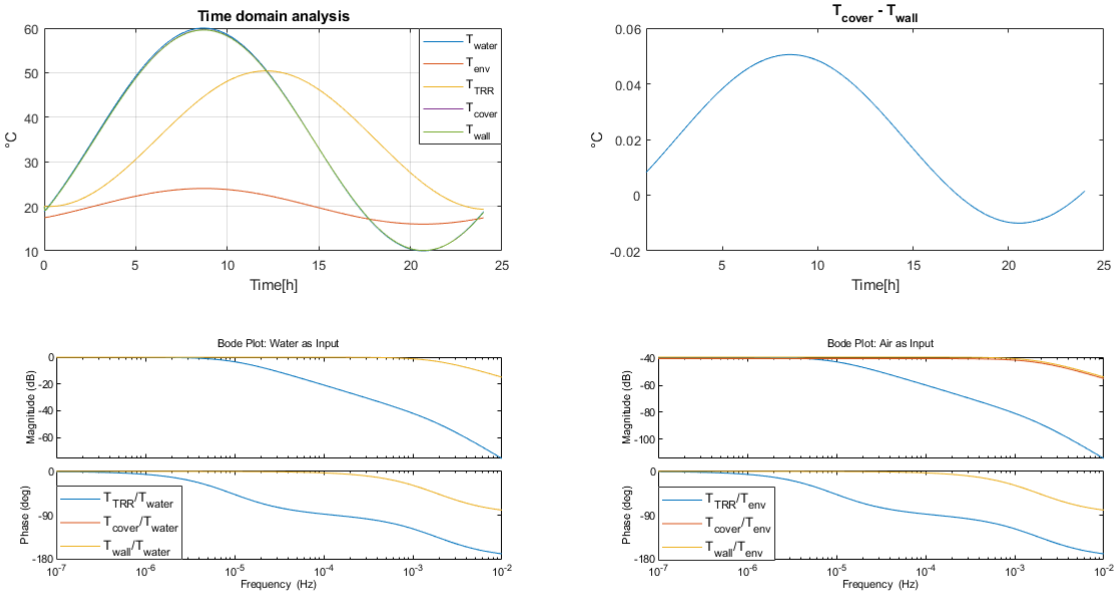

Source: Author

Figure 20 and Figure 21 show the graph of the time domain analysis, which includes the inputs, T_{water} and T_{env}, as well as the outputs T_{wall}, T_{cover}, and T_{TRR}. T_{env} is the environment temperature which represents a disturbance to the system. It will be used to analyze the shielding performance. The wall temperature, the cover temperature and TRR temperature are T_{wall}, T_{cover} and T_{TRR}, respectively. The figures also show the bode plots for T_{water} and T_{env} as inputs. At last, the temperature difference between T_{wall} and T_{cover} is shown to verify the effect of the environmental disturbance in the shield temperature homogeneity.

As expected the wall and cover subsystems have the same dynamic behaviour for T_{water} as an input, since the system was designed for it using Equation 32. This can be seen by the overlap of both transfer functions, $\frac{T_{cover}}{T_{water}}$ and $\frac{T_{wall}}{T_{water}}$. Regarding the coupling between the shield temperature (T_{wall} and T_{cover}) and water temperature, the turbulent region has the best coupling. This can be seen in the frequency domain analysis comparing the cut-off frequency of the turbulent flow $f_{c_{turb}} = 0.0018\ Hz$ with the cut-off frequency of the laminar flow $f_{c_{lam}} = 0.0003\ Hz$. However, this is easier to see in the time domain analysis. Note that, for the turbulent flow, the temperatures T_{water}, T_{wall} and T_{cover} are overlapped or coupled, whereas in the laminar flow T_{water} is decoupled from T_{wall} and T_{cover}.

This is important because a good coupling between the temperature of the shielding and the temperature of the water decreases the calibration time and increases the calibration range. In addition, this decreases the impact of thermal disturbances. Indeed, for the turbulent flow, the disturbance of the environment temperature is attenuated 100 times (-38.9 dB), whereas for the laminar region the same disturbance is attenuated 10 times (-23.5 dB). For this reason, the environment temperature changes the wall and the cover temperatures more easily in the laminar flow than in the turbulent flow. This decreases the temperature homogeneity of the shield in the laminar flow, as the graphs of the temperature difference between the wall and cover show. The maximum temperature difference is 0.28 $^{\circ}C$ for the laminar flow and 0.05 $^{\circ}C$ for the turbulent flow (see Figure 20 and Figure 21).

To summarize, the function of the shield is to be an isothermal temperature source to TRR and to decrease thermal disturbances into TRR. Thus the enhancement of the functions of the shield was done by making the $\tau_{wall} = \tau_{coil}$ which results in an isothermal shield ($T_{wall} = T_{coil}$). In addition, it was noticed that using flow in the turbulent regime results in an attenuation of 100 times in the magnitude of disturbances and also contributes to maintaining the thermal homogeneity of the shield.

8 Mechanical Design

The calibration tool can be divided in three main parts to simplify the description and explanation of the mechanical design: cylinders, cover and foam. The complete calibration tool can be seen in Figure 22. Note that in this figure the calibration tool is opened and closed. In the opened position the cover is gray and in the closed position the cover is yellow in order to differ each situation.

Figure 22 – 3D views of complete drawing of the calibration tool

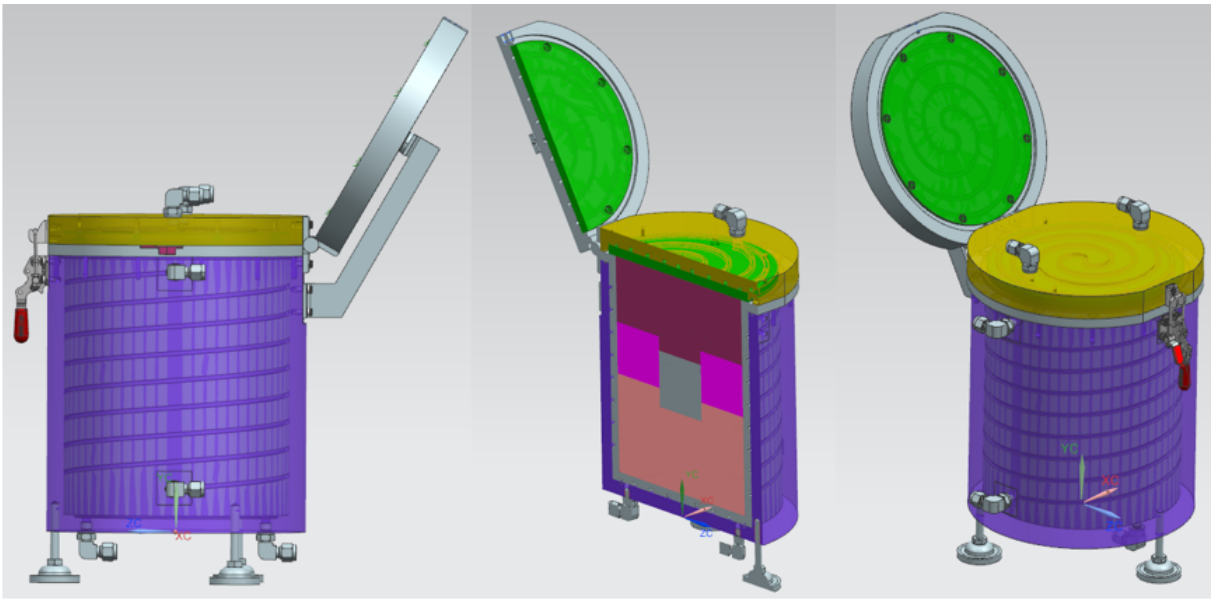

Source: Author

8.1 Cylinders

Figure 23 shows the 3D drawing of the cylinders and all the details mentioned in this paragraph. The spiral and the coil channels must be made inside the shield. To make this, two concentric cylinders have been used. Both channels, spiral and coil, have been designed in the inner cylinder (gray). The channels of the coils can be seen in the outer side of the wall, and the spiral can be seen in the bottom outer side. Regarding the sealing, two O-rings have been used and their grooves can be seen in the outer cylinder. One groove is inside of the cylinder at the bottom. It prevents water from leaking from coil to the spiral. Another groove is at the top to prevent water from leaking to the outside. A little channel in the inner cylinder at the boundary between cylinders and cover has been

made to enable the wires from the sensors to leave the system. It allows the operator to open/close the setup, while minimizing the risk of damaging the wires.

Figure 23 – 3D views of the cylinders

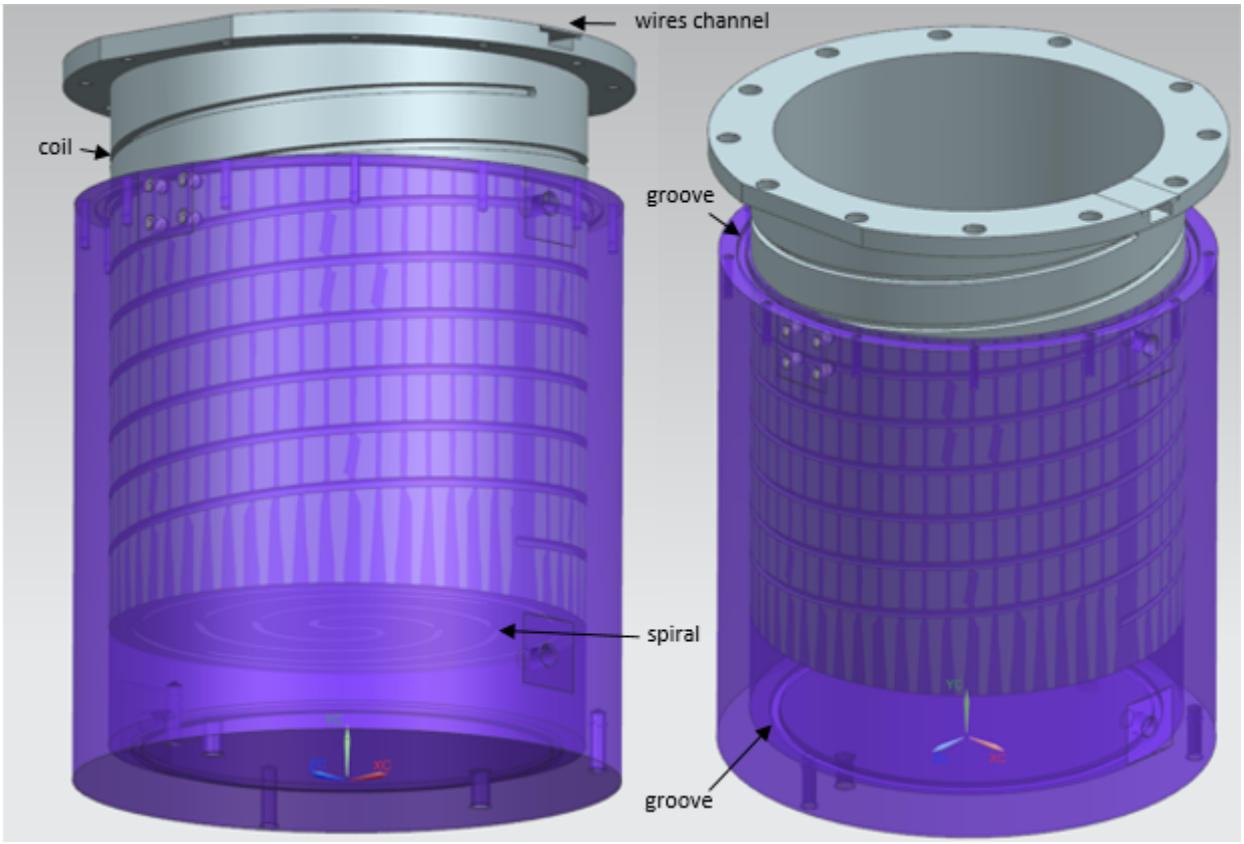

Source: Author

8.2 Cover

Figure 24 shows the 3D drawing of the Cover and the details mentioned in this paragraph. The cover has been designed to be exactly like the bottom-part, such that it keeps the system symmetry when the cover is closed. The cover consists of two parts; the larger part (gray) and the smaller part (green). The larger part contains the spiral's channels and the groove for the O-ring. The smaller part is embedded into the larger part in order to press the O-ring. This embedded design comprises an aesthetic consideration, since the largest face of the larger part stays on the outside. Consequently, the cover seems to be a single piece, see Figure 22. In addition, in the same figure it is possible to see that a support has been mounted onto the cylinders to avoid that the cover opens completely and hits the cylinder. Moreover, this support prevents the set-up from toppling.

Figure 24 – 3D view of the Cover

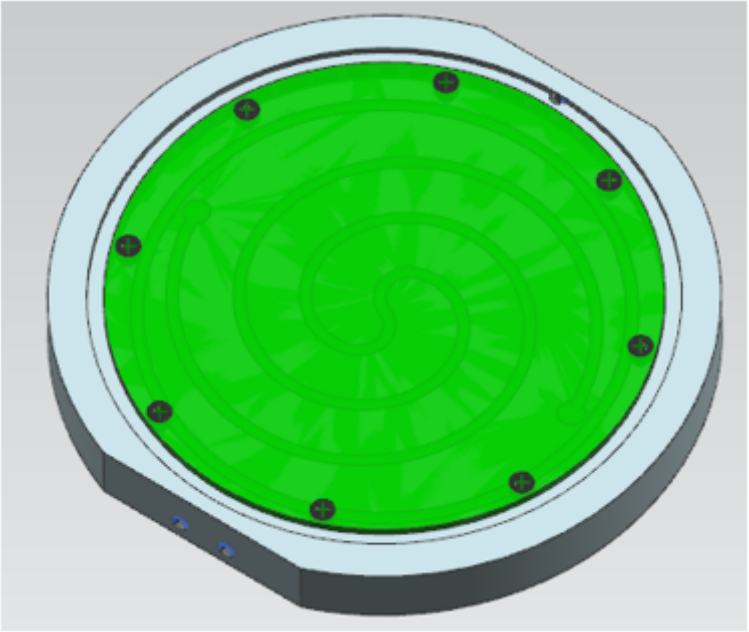

Source: Author

8.3 Foam

Figure 25 shows the 3D drawing of the foam and the details mentioned in this paragraph. The foam is divided in three parts: bottom (rose), middle (pink) and top (purple). The gray cylinder grabbed by the foam is the TRR. The foam works as a support to hold the TRR in the center of the system. For this reason, the bottom part has a hole to place the TRR and ensures its correct positioning at the center of the system. The bottom part ends before the middle of the TRR. It allows the operator to place and remove the cylinder easily. The middle and top part fit in a such a way that a channel, starting from the TRR and ending at the channel between the wall and cover, is created for the wires. The wires leave the frame through this channel.

8.4 Other details

In Figure 24 a groove can be seen between the parts of the cover. This groove was made in the cover to install a small piece of foam. Therefore, when the cover is closed the interface between the cylinders and the cover will be sealed with this foam, avoiding air from flowing into the frame through the interface between the cylinders and the cover.

Figure 25 – 3D view of the foam

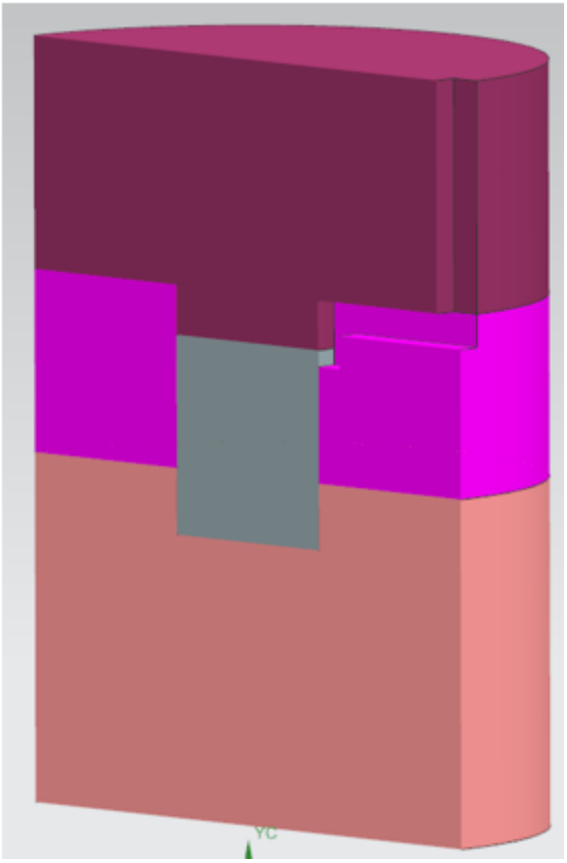

Source: Author

When the foam (Figure 25) is placed inside of the cylinder (Figure 23) it stays 1 mm out of the cylinder. Because of this, when the cover is closed the foam inside the set-up is pressed against the cylinder walls. It ensures that the foam is in contact with the wall and enhances the heat transfer. On the other hand, this makes it necessary to have a clamp to close the system. Finally, three supports are used to elevate the frame in order to create enough space bellow the calibration tool for the water couplings.

9 Conclusion and Comments

The purpose of this project was to develop a high precision temperature sensor calibration tool able to calibrate many contact sensors at the same time. After calibration these sensors can be utilized in the analyses of thermal effects in high precision mechatronics systems. The research covered here encompasses the complete design of the calibration tool, from its conceptual design, passing through its modelling, analyses and optimization. Finally, the 3D drawings have been made for the next phase of the project, which consist of fabrication, assembly, and experimental testing of this setup.

Analysis of the sources of error

Errors due to positioning and conduction via cable were identified as common sources of error for all sensor types. The errors related to conduction via cable are negligible after applying the solution of gluing the cables on the same surface to which the sensor is connected. The high homogeneity achieved during the design of the thermal reference region makes the positioning error negligible as well.

On the other hand, there are no solutions for the SHE and DMME sources of error, since they are inherent to the system. The DMME for NTCs is in the order of milli-Kelvin. For RTD and thermocouples it is tens of milli-Kelvin. Generally, the SHE is smaller than the DMME for all sensors. More specifically, the SHE is smaller for NTCs than for RTDs because of the difference in the operation current used in each sensor (see Tables 2 and 3). Due to the high values of DMME, it is not possible to achieve the requirement of 1 mK for the relative error. However, with the exception of temperatures near 50 $^{\circ}C$, the sensor relative error of NTC50K sensors is smaller than the requirement .

Temperature homogeneity of the thermal reference region

This is the most important aspect in the design since the comparison calibration method requires that the non-calibrated sensor and the reference sensor are at the same temperature. The dilemma is that to obtain a TRR with a highly homogeneous temperature any heat flow into the TRR should be avoided. However, heat flow is necessary to change the TRR temperature in order to perform the calibration in a range of temperatures. For

this reason, just a small portion of heat flow is allowed into the TRR. Moreover, with low heat flow into the TRR, the calibration time increases and the calibration range decreases.

Indeed, the logical reasoning used in the design prioritizes obtaining a high temperature homogeneity in the TRR. As a result, the homogeneity achieved was 0.06 mK/mm, which is almost ten times more homogeneous in temperature than the required 0.5 mK/mm. However, the calibration time takes more than 24 hours and the calibration range is approximately 17 °C - 53 °C (Figure 15). In order to achieve the specified calibration range, it is mandatory to change the coolant. Instead of using cooled water, a solution of 60% of ethylene glycol should be used. This would provide a range for the source temperature of -20 °C to 90 °C. With this coolant, it is easily possible to realize the desired calibration range and to decrease the calibration time.

Optimization

The optimization of the system consisted of enhancing the functions of the shield. This functions are (1) working as an isothermal temperature ($T_{wall} = T_{coil}$) source for the TRR and (2) protecting the TRR against thermal disturbances.

The first function was achieved by designing the cover and wall subsystems with the same dynamic behaviour. This can be seen in the bode plot with water as an input in Figure 20 and Figure 21, where the transfer functions T_{wall}/T_{water} and T_{cover}/T_{water} are overlapped. This was done by solving Equation 32

The second function was analyzed by comparing the impact of the environmental disturbance on the TRR between the turbulent and the laminar flow. In the bode plot, with air as an input in Figure 20 and Figure 21, it was verified that the environmental disturbance is attenuated 100 times in the turbulent flow, whereas in the laminar flow it is attenuated only 10 times. Moreover, these attenuations also affect of the function (1) of the shield. In this sense, the higher attenuation magnitude of the turbulent region enhances the temperature homogeneity of the shield. Due to the smaller effect of environmental disturbances on the cover and wall temperature in the turbulent flow, the difference $T_{cover} - T_{wall}$ is smaller compared to the laminar flow.

In light of all above mentioned results, it is clear that the system should work in the turbulent regime.

Mechanical Design

The 3D drawing of the wall and cover includes the coil and spiral channels. It is important to note that the channels have been considered circular, although in the 3D design they are rectangular. The reasons for this is that a circular shape is more complex to manufacture, and consequently, more expensive. In this sense, the correction given by Equation 6 should be used.

The details of the 3D design of the TRR still need to be finished. This should include a region in which to place the sensor, as near as possible to the the center of the TRR. This will ensure that the sensors are positioned at the same radius of the cylinder. After that, the next steps will be making the 2D drawings for manufacturing, ordering the parts and assembly.

Bibliography

AVX. *NTC Thermistor Products*. 2019. Catalog. Accessed 30/07/2019. Disponível em: <http://catalogs.avx.com/NTC-Thermistors.pdf>. 40

BRYAN, J. International status of thermal error research(1990). Annals of the CIRP, v. 39, n. 2, p. 645–656, 1990. 14

CENGEL, Y. A. *Heat Transfer A practical Approach*. 2. ed. [S.l.: s.n.], 2007. v. 1. 21

DUBBEL. *Handbook of mechanical engeneering*. W. beitz and k-h kuttener. [S.l.]: Springer-Verlag London Ltd., 1994. v. 1. ISBN 978-1-4471-3568-5. 56

INCROPERA et al. *Fundamentals of Heat and Mass Transfer*. 6. ed. [S.l.]: John Wiley and Sons, Inc, 2007. v. 1. ISBN 0-471-45728-0. 21, 22, 24, 30, 31, 36, 38

ISOTECH. *Calibracion de temperatura Desde la industria al ITS-90*. 2004. 20

JCGM. *International vocabulary of metrology – Basic and general concepts and associated terms (VIM)*. 2008. Online. Accessed 07-05-2020. Disponível em: <https://www.iso.org/sites/JCGM/VIM-introduction.htm>. 19, 41, 42

JONG, W. de. *Modelvorming voor foutendeteotie en-diagnoseModel voor iuchtverwarmer en hydraulisch systeem*. Tese (Doutorado) — Delft University of Technology, 2002. 56

KEYSIGHT, T. *34970A Data Acquisition Switch Unit Family*. 2018. Catalog. Disponível em: <https://literature.cdn.keysight.com/litweb/pdf/5965-5290EN.pdf?id=1000031228:epsg:dow>. 39

KOEVOETS, A. et al. Optimal sensor configuring techniques for the compensation of thermo-elastic deformations in high-precision systems. THERMINIC, p. 208–213, 2007. 15

LABFACILITY. *The new labfacility temperature handbook*. 2006. 19, 20

LAKESHORE, C. *Platinum Specifications*. 2019? DataSheet. Disponível em: <https://www.lakeshore.com/docs/default-source/product-downloads/lstc_platinum_l.pdf?sfvrsn=9157869c_5>. 39

LAMERS, R. Report on sig meeting in zurich. *uMIKRONIEK*, v. 56, n. 3, p. 27, 2014. 14

MORANTZ, P. *Precision Temperature Measurement industrial Short Course*. 2016. 18, 19

MORISHIMA, T. *Novel thermal error reduction techniques in temperature domain*. Tese (Doutorado) — Delft University of Technology, 2016. 14, 15

RUIJL, T. *Ultra Precision Coordinate Measuring Machine - Design, Calibration and Error Compensation*. Tese (Doutorado) — Delft University of Technology, 2001. 29, 31, 32, 36

RUIJL, T. Thermal effects in precision system: Design considerations, modelling, compensation and calidation techniques. Diamond Light Source Proceeding, 2011. 25, 31, 44

RUIJL, T. *Thermal Effects in Mechatronic Systems Introduction to modeling techniques: building lump-mass models*. 2012. Company: MI Partners in mechatronic innovation. 27

SMC, C. o. A. *Circulating Fluid Temperature Controller Refrigerated Thermo-chiller*. 2019. Catalog. Disponível em: <http://ca01.smcworld.com/catalog/Chiller-en/mpv/cat43-hrz_en/data/cat43-hrz_en.pdf>. 32

STRANG, P. G. *The Heat Equation and Convection-Diffusion*. 2006. Disponível em: <https://ocw.mit.edu/courses/mathematics/18-086-mathematical-methods-for-engineers-ii-spring-2006/index.htm>. Acesso em: 4 junho 2020. 71

THERMOCOUPLEINFO.COM. *Type J Thermocouple*. 2011. Disponível em: <https://www.thermocoupleinfo.com/type-j-thermocouple.htm>. Acesso em: 30 Julho 2019. 40

TOOLBOX, E. *Specific Heat of common Substances*. 2003. Online. Accessed 30/07/2019. Disponível em: <https://www.engineeringtoolbox.com/specific-heat-capacity-d_391.html>. 39

TOOLBOX, E. *Specific Heats for Metals*. 2003. Online. Accessed 30-07-2019. Disponível em: <https://www.engineeringtoolbox.com/specific-heat-metals-d_152.html>. 39

WHITE, F. M. *Fluid Mechanics*. 7. ed. [S.l.]: McGraw-Hill, 2007. v. 1. ISBN 978-0-07-352934-9. 24

WHITE, F. M. *Fluid Mechanics*. 7. ed. [S.l.]: McGraw Hil, 2009. v. 1. ISBN 978-0-07-352934-9. 55

APPENDIX A – Development of the equation of the average heat coefficient for fluid flow in a pipe

Writing the convection-diffusion equation (STRANG, 2006) for the case of fluid flow in pipe[1], we get

$$\rho c_p \left(\frac{\delta T}{\delta t} + v \nabla T \right) = \nabla . k \nabla T + Q''' \tag{38}$$

where ρ $[kg/m^3]$ is the density of the fluid, c_p $[J/kg°C]$ is the specific heat of the fluid, T $[°C]$ is the temperature of the fluid, k $[W/K.m]$ is the thermal conductivity of the fluid, v $[m/s]$ is the velocity of the fluid and Q''' $[W/m^3]$ describes sources or sinks of heat, termed as heat generation.

The fluid conduction contribution to the heat transfer is negligible compared to the convection contribution ($k \simeq 0$). The interest for the LMM analyses is on steady-state condition $\frac{\delta T}{\delta t} = 0$. Since the temperature changes in the pipe direction (or flow direction), the problem can be simplified to one dimension. Thus, Equation 38 becomes

$$\rho c_p v \frac{dT}{dx} = Q''' \tag{39}$$

Heat generation due to convection can be expressed as well as

$$Q''' = \frac{hA_s}{V}(T_s - T) \tag{40}$$

where h $[W/K.m^2]$ is the convection heat coefficient, A_s $[m^2]$ is the inner surface area of the pipe, V $[m^3]$ is the volume of the pipe, T_s $[°C]$ is the temperature of the surface A_s and T $[°C]$ is the temperature of the fluid. Writing fluid velocity as $v = \phi/A_c$, where ϕ $[m^3/s]$ is flow of the fluid and A_c $[m^2]$ is the cross-section area of the pipe. Then, equating, Equation 39 and Equation 40, we get

$$\frac{\rho c_p \phi}{A_c} \frac{dT}{dx} = \frac{hA_s}{V}(T_s - T) \tag{41}$$

Note that the length of the pipe can be expresses as $L = V/A_c$. Hence, rearranging Equation 41 and considering $T(0) = T_0$, we obtain the following initial value problem

$$\begin{cases} \rho c_p \phi L \frac{dT}{dx} = hA_s(T_s - T) \\ T(0) = T_0 \end{cases}$$

[1] This equation is quite well explained in <https://en.wikipedia.org/wiki/Convection%E2%80%93diffusion_equation>.

which can be solved by integrating factor method and results in

$$T(x) = (T_0 - T_s)e^{-\frac{hA_s}{\rho c_p \phi L}x} + T_s \tag{42}$$

This equation expresses the temperature of the fluid in any location x in the range $0 \leqslant x \leqslant L$. Knowing the temperature of the fluid, it is possible to calculate the total heat transfer rate by convection as

$$\dot{Q}_t = \int_{x=0}^{L} hP(T_s - T(x))dx \tag{43}$$

where the surface area was written as $A_s = \int_{x=0}^{L} Pdx$, where P is the perimeter of the pipe. Solving Equation 43 ,we get

$$\dot{Q}_t = \rho c_p \phi (T_s - T_0)\left(1 - e^{-\frac{hA_s}{\rho c_p \phi}}\right) \tag{44}$$

Using the definition of total heat transfer rate Equation 4 as

$$\overline{h} = \frac{\dot{Q}_t}{A_s(T_s - T_0)} \tag{45}$$

and replacing Eq. 44 in Eq. 45, we obtain the average convection coefficient for fluid flow in pipes

$$\boxed{\overline{h} = \frac{\rho c_p \phi}{A_s}\left(1 - e^{-\frac{N_u k A_s}{d\rho c_p \phi}}\right)} \tag{46}$$

where the convection coefficient h in the Eq. 44 was replaced by $h = N_u k/d$ from the definition of Nusselt number (see Equation 11).